Synthesis and Photophysical Properties of Lanthanide Pyridinylphosphonic Tacn and Pyclen Derivatives: From Mononuclear Complexes to Supramolecular Heteronuclear Assemblies

Nadège Hamon, Léna Godec, Elsa Jourdain, Carlos Platas-Iglesias, Maryline Beyler, Loïc Charbonnière, Raphaël Tripier

Synthesis and photophysical properties of lanthanide pyridinylphosphonic tacn and pyclen derivatives: from mononuclear complexes to supramolecular heteronuclear assemblies

Nadège Hamon,[a,ǂ] Léna Godec,[b,ǂ] Elsa Jourdain,[b] Fátima Lucio-Martínez,[c] Carlos Platas-Iglesias,[c] Maryline Beyler,[a] Loïc J. Charbonnière [b,*] and Raphaël Tripier[a,*]

[a] *Univ Brest, UMR CNRS 6521 CEMCA, 6 Avenue Victor Le Gorgeu, 29200 Brest, France.*
[b] *Equipe de Synthèse pour l'analyse, Institut Pluridisciplinaire Hubert Curien, UMR 7178, CNRS / Université de Strasbourg, ECPM, 25 rue Becquerel, 67087 Strasbourg Cedex 2, France.*
[c] *Centro de Investigacións Científicas Avanzadas (CICA) and Departamento de Química, Universidade da Coruña, Campus da Zapateira-Rúa da Fraga 10, 15008 A Coruña, Spain*

KEYWORDS: azamacrocycle, pyclen, tacn, lanthanide(III), luminescence

ǂ These authors contributed equally

ABSTRACT: Synthetic methodologies were developed to achieve the preparation of ligands **L1** and **L2** consisting in tacn- and pyclen-based chelators decorated with pendant arms consisting in pyridinylphosphonic groups combined with ethylpicolinamide or acetate coordinating functions respectively. Phosphonate functions have been selected for their high affinity towards Ln^{3+} ions compared to their carboxylated counterparts and for their steric hindrance that favors the formation of less-hydrated complexes. Thanks to regiospecific *N*-functionalization of the macrocyclic backbones, the two ligands were isolated with good yields and implicated in a comprehensive photophysical study for the complexation of Eu^{3+}, Tb^{3+} and Yb^{3+}. The coordination behavior of **L1** and **L2** with these cations has been first investigated by means of a combination of UV-vis absorption spectroscopy, steady-state and time-resolved luminescence spectroscopy and ^{1}H and ^{31}P NMR titration experiments. Structural characterization in solution was assessed by NMR spectroscopy corroborated by theoretical calculations. Spectroscopic characterization of the [Ln**L1**] and [Ln**L2**] complexes was done in water and D_2O and showed the effective sensitization of the lanthanide metal-centered emission spectra, each exhibiting typical lanthanide emission bands. The results obtained for the phosphonated ligands were compared to those reported previously for the corresponding carboxylated analogues.

INTRODUCTION

Complexes of the trivalent lanthanide ions (Ln^{3+}) are receiving great attention due to the importance of several applications associated to their magnetic (Gd^{3+}, Dy^{3+})[1-3] and optical (Eu^{3+}, Tb^{3+}, Yb^{3+}, Sm^{3+}, Er^{3+}, Dy^{3+}...) properties.[4-7] Indeed, the paramagnetic Gd^{3+} ion is very efficient in promoting the relaxation of proximate active NMR nuclei, which allowed complexes of this ion to be used in clinical practice as contrast agents in magnetic resonance imaging. Complexes of Dy^{3+} and other lanthanides are being also intensively investigated as single molecule magnets due to their large magnetic anisotropies. Concerning optical properties, the visible emissions of Eu^{3+} and Tb^{3+} ions remain the most exploited in many fields including bioimaging and bioanalysis.[8] However, NIR (Near Infra-Red) emitters (Yb^{3+}, Dy^{3+}, Er^{3+}…) are gaining increasing attention, especially for biological applications.[9] For example, biphotonic Yb(III)-based bioprobes were designed for NIR-to-NIR cell imaging.[10-12] Additionally, the energy migration pathways within Ln^{3+} complexes are of prior importance in applied fields such as the improvement of photovoltaic devices.[13] Understanding the structure/activity relationships associated to the energy transfer processes in Ln^{3+} complexes thus remains an important challenge for the design of supramolecular assemblies able to convert low energy photons in the NIR to Visible emission, thereby generating upconversion (UC). As an example, the full understanding of the assembly processes leading to hetero-polynuclear Yb/Tb systems allowed for the first-time attaining UC at the molecular scale in D_2O[14,15] and in water,[15] where the NIR excitation of the Yb^{3+} center (980 nm) resulted in a cooperative photosensitization of the Tb^{3+} ion as observed by the detection of its characteristic green emission.

It is important to keep in mind that the optimization of the luminescence properties is based on the use of chromophore-containing chelators, which allow the appropriate sensitization of the Ln^{3+} ion through the antenna effect.[16] Additionally, the ligands should lead to thermodynamically and kinetically stable Ln^{3+} chelates, especially for *in vivo* applications, to avoid the release of the Ln^{3+} ion and therefore to prevent toxicity and the extinction of the luminescent properties. Polyazamacrocycles such as tacn (1,4,7-triazacyclononane), cyclen (1,4,7,10-tetraazacyclododecane), pyclen (3,6,9,15-tetraazabicyclo[9.3.1]pentadeca-1(15),11,13-triene) and even

cyclam (1,4,8,11- tetraazacyclotetradecane) are recognized as convenient platforms for the coordination of several metal cations, including Ln^{3+} ions, after functionalization of their amine groups.[17] With some exceptions,[18,19] cyclam-based Ln^{3+} complexes proved to be quite unstable, whereas cyclen-based lanthanide chelates have been the focus of numerous studies and have been probably the most studied for their photophysical properties.[20-23] We and others have largely contributed to the development of cyclen-based ligands for Ln^{3+} complexation, by preparing new specifically *N*-functionalized ligands thanks to efficient synthetic methodologies.[24-26] Tacn-based chelators are also part of the golden standards to afford astonishing optical properties.[15,27-31] Tacn was mostly tri-*N*-functionalized with three identical pendant arms, but compared to the cyclen platform, specific *N*-functionalization is facilitated due to the lower number of amine groups. Derivatives of the 12-membered tetraazamacrocyclic ligand pyclen, which includes a pyridine unit within the ring, have been far less studied.[32,33] We therefore have stepped up our efforts to take advantage of its structure to develop new lanthanide(III) chelates.[34-36] Indeed, the presence of the aromatic moiety confers to the macrocyclic backbone an interesting rigidity that constrains the overall structure, which sometimes leads to uncommon properties when compared to other closely related azamacrocycles. More surprisingly, the regiospecific *N*-functionalization of the pyclen backbone has a deep impact on the physico-chemical and photophysical properties of the Ln^{3+} chelate, with optimal properties being obtained in the case of dissymmetric arrangement of the pendant arms. For example ligand **L** (Chart 1), N^3,N^6-difunctionalized by two picolinate moieties, forms a very stable Tb^{3+} complex (log K_{TbL} = 25.2)[37] characterized by very interesting luminescent properties (ϕ > 95 %, τ = 2.40 ms).[34]

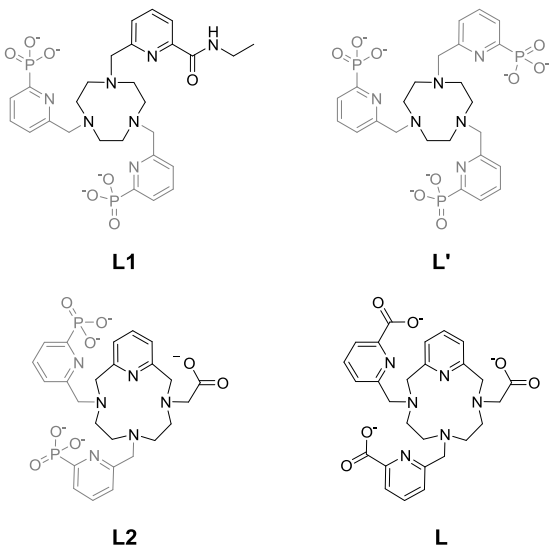

Chart 1. Ligands discussed in this work.

To improve the thermodynamic stability of Ln^{3+} chelates, while favoring radiative de-excitation of the central ion, the picolinate units can be substituted by their phosphonate analogues. Some reports demonstrated that phosphonate functions have a higher affinity with trivalent lanthanide ions compared to their carboxylate counterparts,[38] while the steric compression exercised by the phosphonate groups favors the formation of less-hydrated Ln^{3+} complexes.[39-44] Phosphonate pendants have also the ability to further form electrostatic interactions in presence of an excess of Ln^{3+} ions and to generate discrete polynuclear assemblies.[14,15,41,45] For example, the Yb^{3+} complex obtained from ligand **L'** (Chart 1) is able to interact with Tb^{3+} to give $[(YbL')_2Tb_x]$ (x = 1 or 2) supramolecular assemblies displaying cooperative UC photosensitization in water.[15]

In this work, we aim to explore the photophysical properties of new lanthanide complexes based on macrocyclic scaffolds containing methylpyridin-2-yl phosphonic acid units. We developed the synthetic methodology required to achieve a dissymmetric arrangement of the pendant arms, which allowed the preparation of ligands **L1** and **L2** (Chart 1), *via* regiospecific *N*-functionalization of tacn or pyclen platforms. The coordination behavior of these ligands with Ln^{3+} cations and the photophysical properties of isolated mononuclear complexes is presented. Furthermore, we also analyzed their ability to form supramolecular heteronuclear assemblies that was corroborated by spectroscopic studies and theoretical calculations.

RESULTS AND DISCUSSION

Ligands synthesis. The synthesis of **L1** is described in Scheme 1 and full experimental details are given in the Experimental Section (Figures S1 to S20). Compound **1** was first synthesized in two steps from commercially available 2,6-pyridinedicarboxylic acid according to the literature.[46]

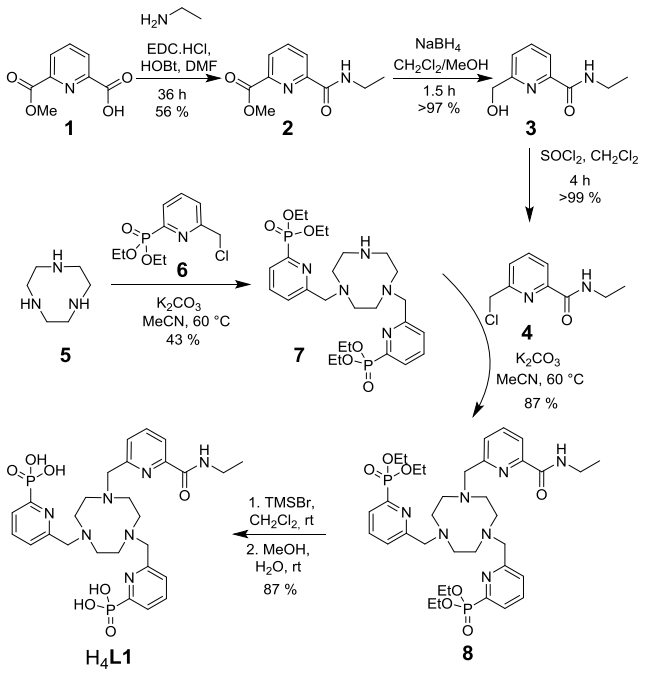

Scheme 1. Synthesis of H_4L1.

Peptidic coupling conditions (HOBt, EDC·HCl in DMF) were chosen to react compound **1** with ethylamine affording compound **2** in 56 % yield. Reduction of the methyl ester moiety to primary alcohol followed by a chlorination reaction in the presence of thionyl chloride led to compound **4** in almost quantitative yield over the two steps. In parallel, alkylation of 1,4,7-triazacyclononane **5** with two equivalents of the pyridine derivative **6**[44] gave compound **7**, along with the formation of the mono- and trisubstituted derivatives. Optimized purification of the mixture by column chromatography on alumina allowed isolating compound **7** in 43 % yield. The *N*-functionalization reaction of the latter with compound **4** afforded precursor **8**. Deprotection of the phosphonic acid functions was then performed under mild conditions thanks to TMSBr in dichloromethane followed by treatment in methanol/water to give the desired ligand **L1** with 87 % yield.

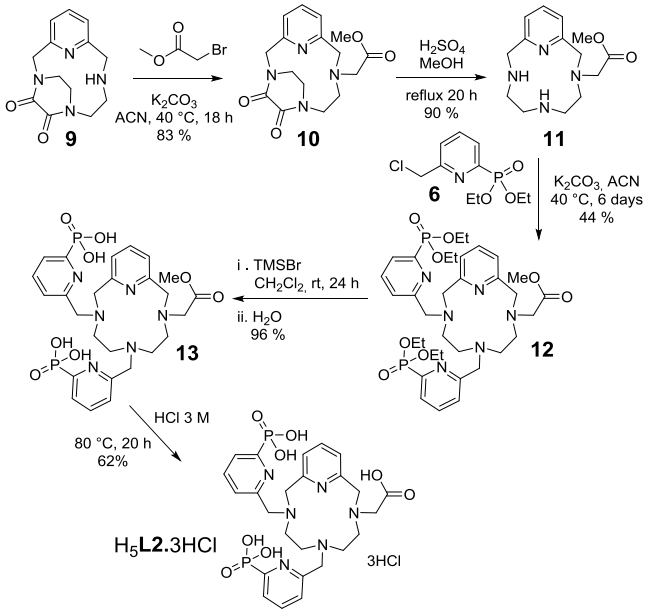

Scheme 2. Synthesis of H_5L2·3HCl.

The synthesis of **L2** (Scheme 2) started from the pyclen derivative **9**, on which two adjacent amine functions of the macrocyclic platform are protected thanks to a diamide bridge.[47] This allowed the N^3-regiospecific functionalization of compound **9** with one equivalent of methyl bromoacetate in 83% yield. Deprotection of the amine functions was then performed with acidic conditions under reflux according to a well-known procedure.[48] *N*-functionalization of the resulting pyclen derivative **11** with two equivalents of compound **6** was followed by TLC and mass spectrometry but turned out to be very slow, requiring six days of reaction at 40 °C to form predominantly trifunctionalized pyclen **12**. The latter was partly retained on alumina during its purification, explaining the moderate yield of this step (44 %). The hydrolysis of both methyl ester and phosphonic esters was first attempted in 3 M HCl at 60 °C for 12 hours, but only a partial deprotection of the phosphonic esters was observed, while increasing the reaction time up to eight days led to the degradation of compound **12**. Therefore, a second strategy based on the deprotection of the phosphonic acids under mild conditions (TMSBr at room temperature for 24h) was adopted, followed by the hydrolysis of the methyl ester in 3 M HCl to yield ligand **L2** as its tri-hydrochloride salt. Full NMR and HRMS characterization of pyclen derivatives **12** and **13** and ligand **L2** can be found in the supporting information (Figures S21-S29).

Spectrofluorimetric and UV-Vis absorption titrations of L1 and L2 with Ln^{3+} ions. The coordination behavior of **L1** and **L2** with lanthanide cations (Ln^{3+} = Eu^{3+}, Tb^{3+}, Yb^{3+}) has been investigated by means of a combination of UV-vis absorption spectroscopy, steady-state and time-resolved luminescence spectroscopy. Spectrophotometric titrations were performed with aqueous solutions of the ligands at pH = 7.3 (0.01 M Tris/HCl), by adding increasing amounts of the metal salt up to 4

equivalents. Figure 1 displays the results obtained from the titration of **L1** by Yb^{3+} monitored by absorption and emission spectrophotometry.

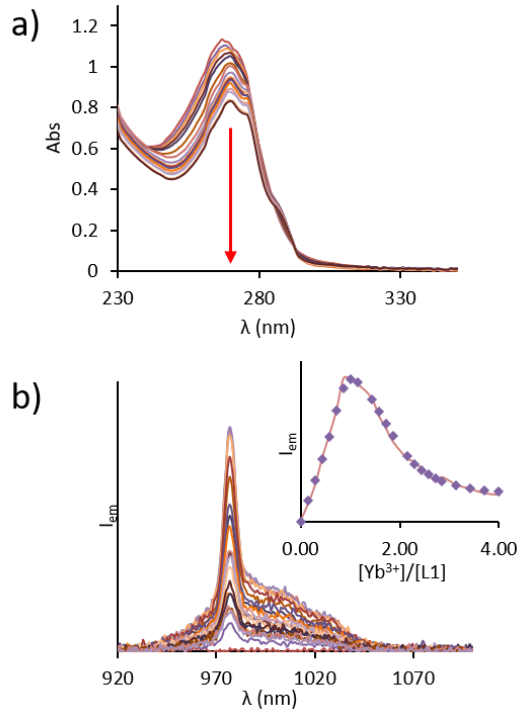

Figure 1. (a) Evolution of the absorption of a solution of L1 (0.76 × 10^{-4} M) upon titration by $YbCl_3 \cdot 6H_2O$ (1.01 × 10^{-3} M) in 10 mM TRIS/HCl, pH = 7.3; (b) Evolution of the luminescence during the titration (λ_{exc} = 268 nm). Inset: Evolution of the total emission intensity as a function of the [Yb^{3+}]/[L1] ratio.

The UV-vis spectrum of the free ligand **L1** exhibits a high energy absorption band centered around 268 nm, characteristic of the π → π* transitions of the aromatic pyridyl rings.[49] Addition of the solution of the Yb^{3+} salt resulted in a bathochromic shift of the maximum from 268 nm to 271 nm (at 1 equivalent) together with the appearance of a shoulder at *ca.* 275 nm, characteristic of the complexation of the aromatic pyridyl phosphonate moieties. Similar results were observed in the case of Eu^{3+} and Tb^{3+} (Figures S30 and S32).

Excitation into the pyridyl phosphonate-centered absorption band at 268 nm upon addition of the Yb^{3+} solution led to the characteristic spectral signature of Yb^{3+} in the NIR, with the emission spectrum displaying the typical emission band due to the $^2F_{5/2} \rightarrow {}^2F_{7/2}$ electronic transition, confirming the antenna effect as responsible for emission sensitization (Figure 1(b)). From 0 to 1 equivalent of Yb^{3+}, the luminescence intensity gradually increased, as a result of the inclusion of the cation into the cavity of the nonadentate ligand. Above one equivalent the luminescence intensity slowly decreased until a plateau was reached. As shown in the inset of Figure 1, the fluorescence intensity as a function of [Yb^{3+}]/[**L1**] ratio shows a marked inflection point for one equivalent, suggesting the formation of a mononuclear complex with high stability constant. After 1 equivalent, changes in the shape of the transition evidence the formation of polynuclear species, which were also observed during the titration with Eu^{3+} and Tb^{3+} (Figures S30 and S32).

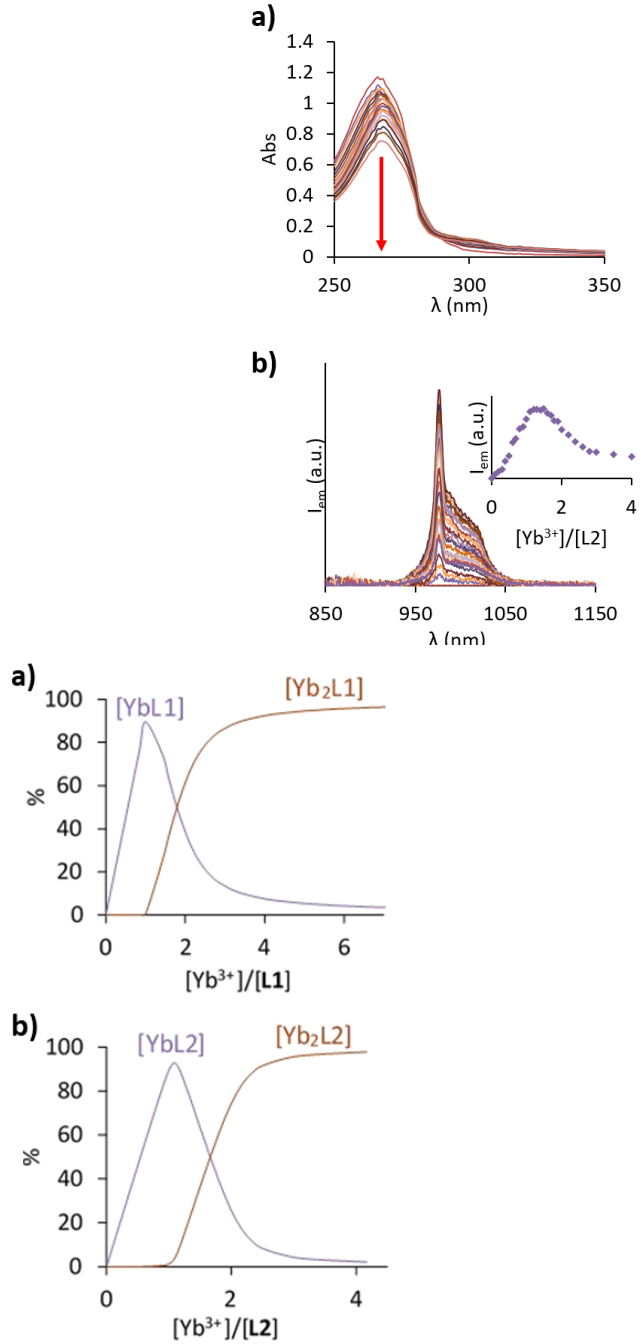

Figure 2. Speciation diagram of the species formed upon addition of $YbCl_3 \cdot 6H_2O$ to (a) an aqueous solution of L1 (10 mM TRIS/HCl, pH = 7.3, λ_{exc} = 268 nm) and (b) an aqueous solution of L2 (10 mM TRIS/HCl, pH = 7.3, λ_{exc} = 268 nm). Charges are omitted for clarity.

The analysis of absorption and emission titration experiments upon addition of Yb^{3+} was performed by using the Specfit software (Figure 2).[50,51] Unfortunately, the sharpness of the inflection points precludes the determination of the association constant for the formation of the Ln**L1** species, pointing to the formation of very stable species ($Log K_{cond} > 7$). The different titrations evidenced the formation of polynuclear species which were ascribed to $[Ln_2$**L1**$]$ entities for Yb and Tb, but interestingly, the careful examination of the $^5D_0 \rightarrow {}^7F_0$ transition of Eu^{3+} (Figure S31b) also evidenced the formation of a $[Eu_3($**L1**$)_2]$ compound. Thus, it is to be kept in mind that the 2:1, Ln^{3+}:**L1** ratio observed for the polynuclear species might reflect the formation of more complex entities such as a $[Ln_{2x}($**L1**$)_x]$ complexes (x = integer). The emission spectrum of the mononuclear complex [Eu**L1**] remains constant on a rather wide range of pH values from ca. 12.0 to 7.5, while below this pH the emission intensity decreases slightly as a consequence of the protonation of the phosphonate groups with an apparent pK_a value of 5.7 (Figure S35). Thus, the complex of **L1** is nearly fully deprotonated at the pH values used for spectroscopic studies.

Similar trends were also obtained in the case of the titration of **L2** with Eu^{3+} and Yb^{3+} (Figures S36 and figure 3). The free ligand **L2** displays a broad absorption band with a maximum at *ca*. 266 nm that is displaced to 267 nm after addition of Ln^{3+} salt. The emission spectra, specific to each lanthanide ion, is observed after progressive addition of the metal solution. In the case of Eu^{3+}, the fluorescence intensity as a function of $[Eu^{3+}]/[$**L2**$]$ ratio shows a marked inflection point for 1 equivalent (Figure S36(a), inset), suggesting as for **L1**, the formation of a mononuclear complex. In the luminescence spectra of a solution of **L2** in the presence of increasing amount of Yb^{3+}, a broad emission band shoulders the sharp $^2F_{5/2} \rightarrow {}^2F_{7/2}$ emission band (Figure 3).

Figure 3 : (a) Evolution of the absorption of a solution of L2 (1.18×10^{-4} M in 10 mM TRIS/HCl) upon titration by $YbCl_3.6H_2O$ (0.98×10^{-3} M, in 10 mM TRIS/HCl, pH = 7.4). (b) Evolution of the luminescence of the solution during the titration (λ_{exc} = 268 nm). Inset: Evolution of the total emission intensity as a function of the $[Yb^{3+}]/[$L2$]$ ratio.

^{1}H and ^{31}P NMR. To get further insights into the coordination properties of the ligands with lanthanide cations, we conducted an NMR titration of **L1** with Lu^{3+}. ^{1}H and ^{31}P NMR spectra, displayed respectively in Figures 4 and 5, were recorded after each addition of an aliquot of metal salt from 0 to 3 equivalents, followed by pD equilibration to 7.0 by addition of NaOD. As Lu^{3+} is added, the ^{1}H signals belonging to the free ligand gradually disappear, while a new set of peaks is observed, corresponding to the formation of the mononuclear complex (between 0.1 and 0.9 equivalents). At 1 equivalent a single set of signals is observed in the ^{1}H NMR spectrum (Figure 4), which shows that the effective C_s symmetry of the free ligand is lost, in agreement with a coordination of the cation in the cavity formed by **L1** and a concomitant wrapping of the arms around the metal leading to Δ and Λ enantiomers.[52]

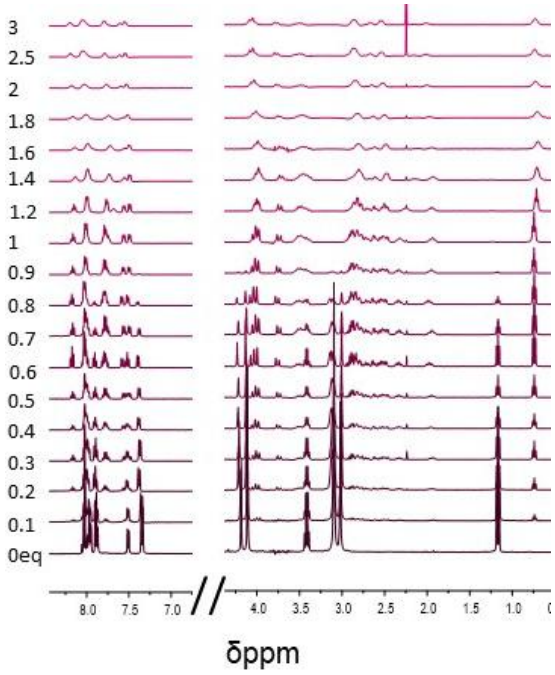

Figure 4. ^{1}H NMR spectra of ligand L1 upon addition of 0 to 3 equiv. of $LuCl_3 \cdot 6H_2O$ (D_2O, pD = 7.0, 298 K, 400 MHz).

The C_1 symmetry also indicates a slow interconversion of the isomers on the NMR timescale. Further additions of aliquots resulted in the broadening of the signals indicating the formation of polynuclear species. ^{31}P NMR also supported the formation of the mononuclear complex up to addition of 1 equivalent of Lu^{3+} (Figure 5), with a strong deshielding of the ^{31}P peak of the free ligand, characteristic of the coordination of pyridyl phosphonate moieties. Furthermore, two new signals are observed, as expected for the formation of the Δ and Λ enantiomers. The large downfield shifts of the peaks upon coordination of the Lu^{3+} cations also indicated that the complexation is accompanied by the second deprotonation of the phosphonate functions.[53,54] After 1 equivalent, as it could be seen for ^{1}H NMR, broad signals are observed, confirming the formation of polynuclear species in slow to intermediate exchange within the timescale of the NMR experiments.

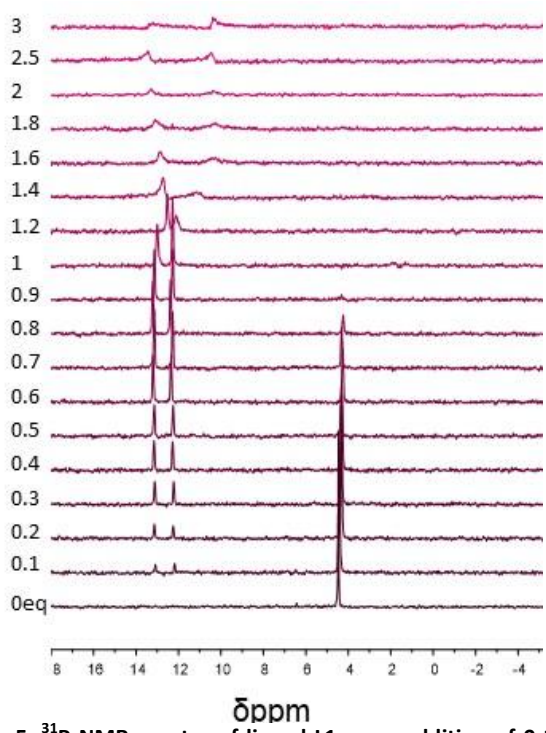

Figure 5. ^{31}P NMR spectra of ligand L1 upon addition of 0 to 3 equiv. of $LuCl_3 \cdot 6H_2O$ (D_2O, pD = 7.0, 298 K, 162 MHz).

Synthesis of the complexes. Synthesis of mononuclear complexes with various lanthanide cations (Eu^{3+}, Tb^{3+}, Yb^{3+}, Lu^{3+}), was undertaken for **L1** and **L2** (Scheme 3). In the case of **L1**, formation of its Ln^{3+} complexes was monitored by ^{1}H and ^{31}P NMR (D_2O, pD adjusted between 6.5 and 7 between each aliquot) to ensure the exact stoichiometry leading to the formation of mononuclear complexes. Complexes were then purified by reverse phase chromatography on a C_{18} column using TFA in the eluents, thus leading to protonated complexes, which were characterized by ^{1}H and ^{31}P NMR, elemental analysis and ESI mass spectrometry (Figure S39-S51). Complexation of ligand **L2** with various lanthanide(III) ions was performed in H_2O at pH ~ 6. After completion of the complexation reaction, desalting by dialysis gave complexes [Ln**L2**] (Ln = Eu, Tb, Yb, Lu) with yields ranging from 67 % to 100 %. All the final complexes were characterized by HRMS and their purity was controlled by analytical HPLC (see Supporting Information, Figures S52-S63). NMR experiments were performed on the diamagnetic [Lu**L2**] chelate. A single set of signals were obtained for ^{1}H, ^{13}C and ^{31}P NMR spectra (Figures S52-S54). In order to investigate the formation of mononuclear entities, a ^{1}H DOSY experiment was recorded in D_2O (pD = 5) for [Lu**L2**] (Figure S55). A diffusion coefficient D_{D_2O} = 2.37 × 10^{-10} $m^2 \cdot s^{-1}$ was measured that corresponds to a Van der Waals radius r of 7.5 Å according to the Stokes-Einstein equation (I) where k_B is the Boltzmann constant (1.38065 × 10^{-23} $J \cdot K^{-1}$), T the absolute temperature (in K) and η the viscosity of the medium (η_{D2O} = 1.232 × 10^{-3} Pa.s at 298 K).[55,56]

$$D = \frac{k_B T}{6\pi r \eta} \quad \textbf{(I)}$$

The diffusion measured in D_2O is somewhat higher than those reported for small mononuclear Ln^{3+} complexes (3.9-5.4 × 10^{-10} $m^2 \cdot s^{-1}$).[57-59] DFT calculations were also used to estimate the molecular volume of [Lu**L2**], which turned out be 678 $Å^3$, as defined by a contour of electron density of 0.001 e·$Bohr^{-3}$ (Table S3). This molecular volume corresponds to that of a sphere with a radius of 5.5 Å. This value is considerably lower than that estimated from diffusion measurements. However, lanthanide complexes with ligands containing phosphonate groups are well-known for having a well-defined second-sphere hydration shell, which may increase the hydrodynamic radius of the complex,[60-62] though some degree of aggregation cannot be excluded.

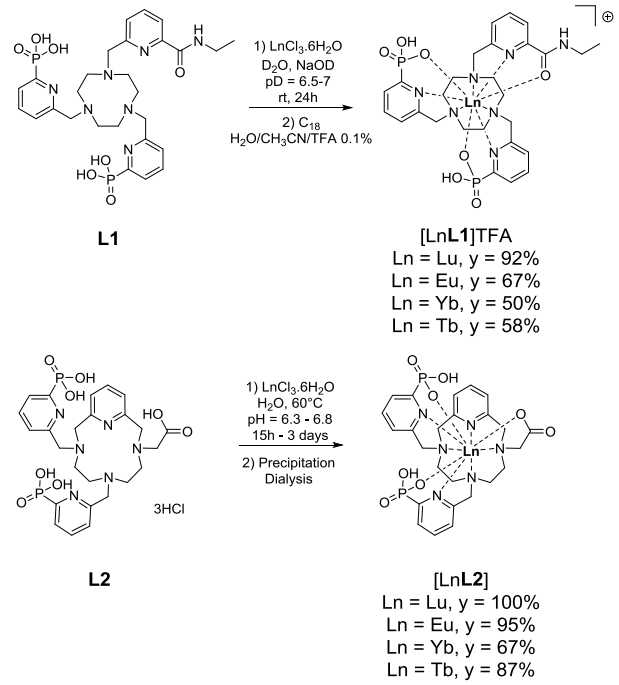

Scheme 3. Synthesis of the [LnL1]TFA and [LnL2] complexes.

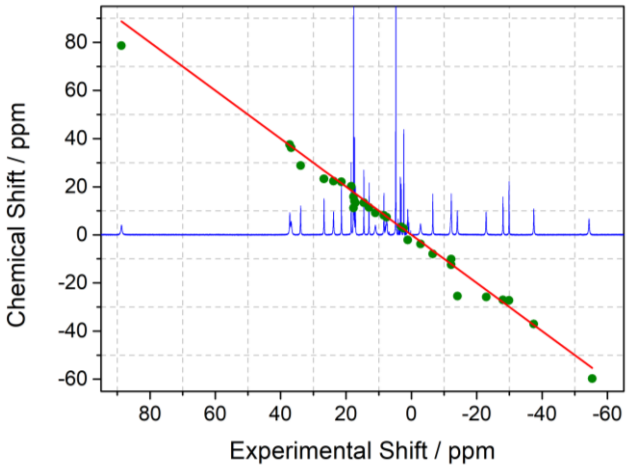

Figure 6: ^{1}H NMR spectrum of the Yb(III) complex of L1 (400 MHz, 298 K, D_2O, pD = 7.0) and comparison of the experimental and calculated shifts. The solid line represents the identity line.

Table 1. Main Spectroscopic Parameters of the [YbL], [TbL], and [EuL] Complexes (L = L1 or L2) in H_2O and D_2O at pH = 7.2.

Species	λ_{exc} (nm)	ε_{H_2O} ($M^{-1}.cm^{-1}$)	ϕ_{H_2O}(%)	ϕ_{D_2O}(%)	τ_{H_2O} (µs)	τ_{D_2O} (µs)	q
[Eu**L1**]$^-$	268	12 560	12	13	1160	1720	0
[Tb**L1**]$^-$	268	11 270	40	55	2470	2620	-0.2
[Yb**L1**]$^-$	268	12 000	0.3	1	3.4	11.1	-0.1 – 0.1
[Eu**L2**]	270	11 910	20	31	1380	2025	0
[Tb**L2**]	270	12 870	61	81	1960	2450	0.2
[Yb**L2**]	270	12 050	0.3	2	3.8	13.8	-0.1-0.1

At neutral pD, the [Yb**L1**]$^-$ complex displays a rather well resolved ^{1}H NMR spectrum, with 30 paramagnetically shifted signals spread over the approximate 90 to -60 ppm range. These signals could be assigned on the basis of their linewidths, relative integration and the cross-peaks observed in the COSY spectrum (Figure S47 and Table S1). The paramagnetic shifts were subsequently analyzed assuming that they are dominated by the pseudocontact contribution, following the methodology applied to other Yb^{3+} complexes.[63] The analysis of the paramagnetic shifts was performed by using the structure of the complex optimized using DFT calculations, which reveals nine coordination of the ligand to the metal ion, as would be expected (Figure S68). All attempts to fit the paramagnetic shifts to the pseudocontact model however failed, as they provide unacceptable deviations of the experimental and calculated shifts. We hypothesized that this may be related to the high negative charge of the phosphonate functions, which results in an optimized geometry where the metal ion is pulled towards the phosphonate groups due to their high negative charge. This effect is expected, given the limitations of continuum models of solvation to account for hydrogen bonding interactions involving the phosphonate groups and solvent water molecules, which leads to an overestimation of electrostatic interactions.[64] This effect is even more pronounced when calculations are performed in the gas phase. To test this hypothesis, we performed calculations on the [YbH_2**L1**]$^+$, in which the phosphonate groups are protonated. Upon protonation, the average Ln-N distances involving amine N atoms shorten from 2.711 to 2.651 Å, as the metal ion approaches the macrocyclic mean plane. The protonated complex provides a reasonably good fit of the paramagnetic shifts (Figure 6 and table S1), indicating that the structure of the complex in solution is described rather well by this structure, a maximum deviation of calculated versus experimental data of 13.7 ppm and a mean deviation of 5.6 ppm. These deviations are relatively small compared with the overall chemical shift range of the ^{1}H NMR signals of ~143 ppm, though somewhat better agreements were observed for rhombic complexes with a comparable number of signals. This appears to reflect the difficulties in modeling the structures of phosphonate complexes for the reasons outlined above.[65]

The results of the fits provided the parameters D_1 = 2112 ± 126 and D_2 = 1072 ± 214 ppm Å^3, which are proportional to the axial and rhombic parts of the magnetic susceptibility tensor. The values of D_1 and D_2 indicate that the paramagnetic shifts are dominated by the axial contribution, but display a significant contribution from the rhombic term. Furthermore, the main symmetry axis of the magnetic susceptibility tensor (the z axis) is nearly orthogonal with respect to the pseudotrigonal axis (Figure S68). A similar situation in which the easy axis of magnetization is perpendicular to the pseudotetragonal axis was observed for [Dy(DOTA)]$^-$.[66]

Spectroscopic characterization of the [LnL] complexes. The UV-visible spectra of all complexes ([Ln**L**], Ln = Eu, Tb, Yb, **L** = **L1**, **L2**) were measured in water and D_2O and exhibit, in both solvents, a strong absorption band centered at *ca.* 268 nm together with a shoulder at *ca.* 275 nm (Figure 7), as already observed during spectrophotometric titrations of ligand **L1** with Ln^{3+} (Figure 1). As expected, the excitation spectra (Figure 7) recorded on the metal-centered emission overlap very well with the absorption spectra, indicating the energy transfer from the ligand to the metal as a result of the antenna effect. Upon excitation of the complexes into the ligand absorption bands at 268 nm, effective sensitization of the lanthanide and metal-centered emission spectra were observed, exhibiting each typical lanthanide emission bands, corresponding to the $^5D_4 \rightarrow {}^7F_J$ (J = 6 to 3) transitions for Tb^{3+}, the $^5D_0 \rightarrow {}^7F_J$ (J = 0 to 4) for Eu^{3+} and to the $^2F_{5/2} \rightarrow {}^2F_{7/2}$ transition for Yb^{3+} in the NIR domain as displayed in Figure 7. Similar trends were observed for [Ln**L2**] complexes upon excitation at 268 nm (Figure S65).

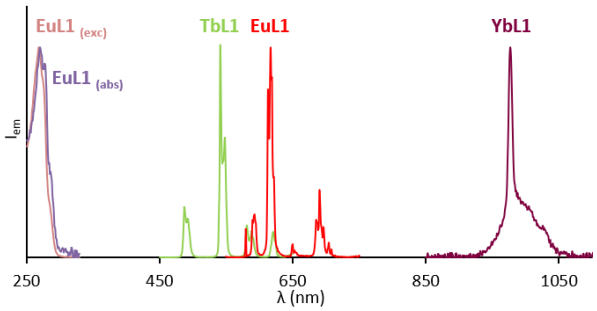

Figure 7. UV/vis absorption (brown) and excitation (pink) spectra of [EuL1] (left) and normalized emission spectra (λ_{exc} = 268 nm) of a H_2O solution of [LnL1]TFA with Ln = Yb (purple), Eu (red) and Tb (green) (right).

The main spectroscopic properties measured for the [Ln**L**] (**L** = **L1**, **L2**) complexes (Ln = Eu, Tb, Yb), in water and in D_2O, are presented in Table 1. The spectroscopic results observed from the study of the complexes obtained with three different Ln^{3+} ions reveal several interesting properties. First, the hydration number, calculated with the luminescence lifetimes in water and in D_2O according to the methodology developed by Beeby and co-workers[67] confirms the nonadentate coordination of the ligand with lanthanides having no inner-sphere water molecule. In all cases, luminescence lifetime measurement indicated a decay perfectly fitted with mono-exponential functions. The overall luminescence quantum yields were measured in water and D_2O. In the case of Tb^{3+}, results are rather similar to data reported for complexes based on tacn with phosphonated pyridine arms (Ligand **L'**, Chart 1),[44] while in the case of europium(III) the values are rather high compared to previous results. In the case of the lanthanide(III) complexes of **L2**, opposite trends are observed. While quite similar luminescent properties in water are observed when comparing [Eu**L1**] (Chart 1) and [Eu**L2**], both the luminescence quantum yields and lifetimes are significantly decreased for [Tb**L2**] compared to its carboxylated analogue [Tb**L**] (respectively 2400 µs and 90 % for the excited state lifetime and quantum yield of [Tb**L**]).[34]

Finally, it is important to draw attention on the lifetimes of the ytterbium complexes in water and in D_2O. These values are identical for the Yb complexes of **L1** and **L2**, both containing two phosphonated pyridine pendants. These results underline the efficiency of such coordinating arms to sensitize the luminescent of Yb^{3+}. Interestingly, the values are rather similar, even higher, to those already observed in our group for complexes that led to upconversion in water.[15]

Luminescent titrations of the [Tb**L1**]$^-$ complex with increasing amounts of Eu^{3+} were performed (Figures S64(b) and (c)). Upon addition of increasing amounts of Eu^{3+}, a progressive decrease in the Tb^{3+}-centered emission was observed, accompanied by the increase of the typical Eu^{3+}-centered bands at lower energies (ca. 700 nm). The fluorescence intensity as a function of [Eu^{3+}]/[Tb**L1**] decreases exponentially until an equimolar mixture of Eu^{3+} and [Tb**L1**]$^-$ is obtained, then a plateau is reached and the emission remains constant despite the addition of additional Eu^{3+} (Figure S64(c)). As proven by previous work,[41] the decrease of Tb^{3+}-centered luminescence comes from intermetallic *f–f* energy transfer, meaning formation of polynuclear species and not from metal exchange in the macrocyclic cavity. Indeed, the theorical speciation diagram obtained based on this titration indicates the formation of two new species. With a ratio [Eu^{3+}]/[Tb**L1**] lower than 1, the [Tb**L1**]$^-$ monomer coexists with [Eu(Tb**L1**)$_2$]. With higher ratios, [Eu_2(Tb**L1**)$_2$] is predominant (Figure S64(a)). In the case of **L2** a similar behavior is observed, the luminescence of [Tb**L2**] decreases upon addition of Eu^{3+} (Figure S66(b)). However, when reporting luminescence intensity according to [Eu^{3+}]/[Tb**L2**], the Tb^{3+}-emission intensity decreases dramatically until this ratio is equal to 0.5, then it decreased slowly until it reached a plateau (Figure S66(c)). The calculated speciation diagram indicates in this case the formation of the polynuclear [Eu(Tb**L2**)$_3$] species with low concentrations of Eu^{3+} and [Eu_x(Tb**L2**)$_x$] (x = integer) is quantitively formed from equimolar mixture of Eu^{3+} and [Tb**L2**] (Figure S66(a)).

Computational studies. The absorption and emission spectra of the [Yb**L1**] complex was further analyzed using theoretical calculations with the *N*-electron valence state perturbation theory (NEVPT2) method, which incorporates dynamic correlation on the top of the CASSCF wave function (see computational details below). Given the results obtained from the analysis of the Yb^{3+}-induced paramagnetic shifts, we used in this calculations the deprotonated from of the complex. Spin-orbit coupling effects were incorporated using quasi-degenerate perturbation theory. The $^2F_{7/2}$ ground state of Yb^{3+} splits into four Kramer's doublets by effect of the ligand crystal field (levels 0 to 3 in Table 2), while the $^2F_{5/2}$ level splits into three Kramer's doublets (levels 4 to 6). The experimental absorption and emission spectra (Figure 8) are dominated by a sharp feature at 977 nm that can be assigned to the 4↔0 transition on the basis of CASSCF/NEVPT2/QDPT calculations, which predict this transition at 987.8 nm (Table 2).

The absorption spectrum displays two shoulders on the high-energy side at around 963 and 947 nm that can be attributed to the 5←0 and 6←0 transitions, respectively. The three transitions observed in the absorption spectrum provide the splitting of the excited $^2F_{5/2}$ level. The deconvolution of the emission spectrum using Gaussian functions (Figure S70), provided estimates of the 4→1, 4→2 and 4→3 transitions, which are observed at 983, 1004 and 1021 nm. The agreement between the experimental and calculated data is rather good, with the calculated absorption spectrum being very similar to the experimental one, though slightly shifted to lower energies (Figure S69). The mean deviation between the experimental absorption and emission data and the calculated transitions amounts to 115 cm^{-1}. Noteworthy, the simulations of the absorption spectrum required using different linewidths for the dominant 4←0 transition (40 cm^{-1}) and the remaining transitions (400 cm^{-1}). This is in line with the deconvolution of the experimental spectrum using Gaussian functions, which evidences that the 4←0 transition is considerably sharper than the remaining components (Figure S70).

Table 2. Experimental absorption and emission spectral data obtained for the [YbL1] complex and results obtained with CASSCF/NEVPT2/QDPT calculations.

Transition (pop.)[a]	λ (nm)	Energy (cm^{-1})	$10^9 \times f_{osc}$	Exp (nm)[c]	Exp (nm)[d]
4↔0 (0.504)	987.8	10123.7	272	978	977
5↔0 (0.504)	974.5	10261.6	110	963	
6↔0 (0.504)	958.1	10437.4	74	947	
4↔1 (0.268)	1000.8	9992.1	70		983
5↔1 (0.268)	987.2	10130.0	76		
6↔1 (0.268)	970.3	10305.7	98		
4↔2 (0.154)	1012.6	9875.7	36	1024	1004
5↔2 (0.154)	998.6	10013.6	44		
6↔2 (0.154)	981.4	10189.4	14		
4↔3 (0.074)	1028.5	9722.5	8		1021
5↔3 (0.074)	1014.2	9860.4	14		
6↔3 (0.074)	996.4	10036.1	2		

[a] Boltzmann population of the lowest energy level involved in the transition at 300 K provided within parentheses. [b] Data from absorption spectra. [c] Data from emission spectra.

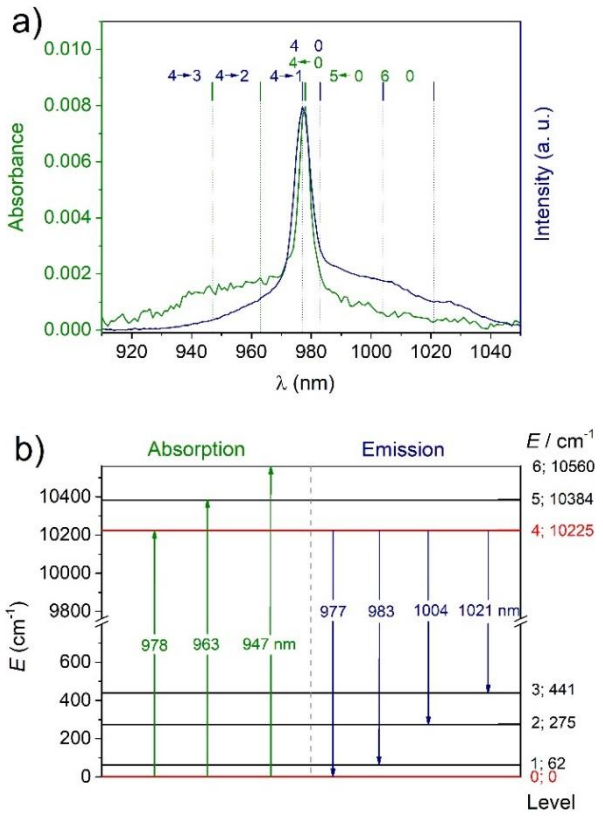

Figure 8. a) UV/vis absorption (green) and emission (blue) spectra of $[YbL1]^+$ and b) Energy diagram obtained from the analysis of the spectral data, with each horizontal line representing a Kramer's doublet.

The overall splitting of the $^2F_{7/2}$ level (441 cm^{-1}) is quite small compared with other Yb^{3+} complexes, which display twice as high energy differences between the lowest and highest energy Kramer's doublets of the $^2F_{7/2}$ manifold.[68,69] This appears to be related to the tricapped trigonal prismatic coordination environment around the metal ion, which is characterized by small crystal field splitting effects.

CONCLUSION

Polyazacycloalkanes are very interesting coordinating macrocyclic platforms to form highly stable complexes with several cations and, once *N*-functionalized, can afford very powerful ligands for the coordination of trivalent lanthanides cations. If cyclen-based chelators have been probably the most employed in the literature to form Ln-complexes for several applications including luminescence, tacn and pyclen derivatives that were less studied a decade ago have proved their ability to contribute to the building of numerous π-acceptor ligands for development of luminescent complexes. We and others have for instance developed some bioprobes based on these azamacrocycles[27,28,29,31,34,35,36] and also demonstrated interesting up conversion behaviors to produce high energy emission photons.[15] In this study we first succeeded in synthesizing two new ligands **L1** and **L2** in tacn- and pyclen-based chelators with a dissymmetric arrangement of the pendant arms consisting in respectively pyridinylphosphonic groups combined with ethylpicolinamide or acetate coordinating functions, respectively. Our previously developed regiospecific functionalizations were then employed with new pendants highlighting their versatility. Prior to the complexes synthesis, the coordination of **L1** and **L2** with Eu^{3+}, Tb^{3+} and Yb^{3+} has been investigated by means of a combination of UV-vis absorption spectroscopy, steady-state and time-resolved luminescence spectroscopy and ^1H and ^{31}P NMR. Then, spectroscopic characterization of the synthesized complexes was performed in water and D_2O. Experiments clearly demonstrated the formation of the usual 1:1 **L**:Ln species but also polynuclear adducts with a 1:2 ratio. Very interestingly trends can be highlighted with opposite behaviors of the Tb^{3+} and Eu^{3+} complexes of **L1** and **L2** compared to their previous carboxylated derivatives, but the important information was given by the ytterbium complexes. Indeed, their long excited state lifetimes in water and in D_2O underlined the efficiency of such two phosphonated pyridine pendants to sensitize the luminescence of Yb^{3+}. Finally, calculations were achieved and unambiguously confirmed the experimental data obtained by ^1H-NMR for the structure and by spectroscopy for the absorption and emission properties, further supporting our conclusions.

EXPERIMENTAL SECTION

Materials and methods. Reagents were purchased from ACROS Organics and from Aldrich Chemical Co and used without further purification. Dialysis membranes (cut-off 100-500 Da) were purchased from Repligen. All solvents were dried and distilled prior to use according to standard methods. Compound **1**,[46] compound **6**[15,70] and pyclen derivative **11**[48] were synthesized according to previous procedures. Analytic HPLC analyses were performed on a Prominence Shimadzu HPLC/LCMS-2020 equipped with a UV SPD-20 A detector. The chromatographic system employs a HPLC Column (Puriflash Prep C_{18AQ} 5 µM 250×4.6 mm) with H_2O (+ 0.1% TFA or HCOOH) and MeOH or CH_3CN as eluents (gradient detailed under each chromatogram in the supporting information) at a flow rate of 1 mL/min and UV detection at 254 and 350 nm. NMR spectra were recorded at the "Services communs" of the University of Brest or at the University of Strasbourg. ^1H and ^{13}C NMR spectra were recorded using Bruker Avance 500 (500 MHz), Bruker Avance 400 (400 MHz), or BrukerAMX-3 300 (300 MHz) spectrometers. Chemical shift (δ) values are given in parts per million and are referenced to the solvent.[71] The given pH values are corrected for the deuterium isotopic effects (pD = apparent pH + 0.4).[72] When attribution of the NMR signals is done in the experimental part (according to 2D NMR experiments), labelling of the molecules is given in the supporting information. HRMS analyses were realized on a HRMS Q-Tof MaXis, sources ESI, APCI,

APPI, nano-ESI (at the Institute of Organic and Analytic Chemistry – ICOA in Orléans). Elemental analysis and mass spectrometry analysis were carried out by the "Service Commun d'Analyses" of the University of Strasbourg and analyzed using the ChemCalc Software.[73]

Synthesis. *6-(Methoxycarbonyl)picolinic acid (**1**).* Dimethyl pyridine-2,6-dicarboxylate (2.0 g, 10.25 mmol, 1.0 equiv.) was suspended in MeOH (120 mL). The reaction was heated to 50°C until homogenous. 1 M $NaOH_{(aq)}$ (9.74 mL, 9.74 mmol, 0.95 equiv.) was added and the reaction was stirred at 50°C for 15 minutes. The reaction was cooled down to ambient temperature and MeOH concentrated to *ca*. 30 mL and extracted with CH_2Cl_2 (4 × 50 mL). The organic layer was discarded. The aqueous phase was acidified with a 12 M $HCl_{(aq)}$ solution (811 µL, 9.74 mmol, 0.95 equiv.), extracted with EtOAc (4 × 100 mL) and the combined organic layers were dried over $MgSO_4$. The solvent was removed *in vacuo* to give compound **1** as a white solid (1.63 g, 9.00 mmol, 93%). ^{1}H NMR (400 MHz, 298 K, $(CD_3)_2SO$): δ 13.48 (s, 1H, $CO_2\underline{H}$), 8.26-8.21 (m, 2H, 2 × Py$\underline{H}$), 8.19-8.14 (m, 1H, Py$\underline{H}$), 3.91 (s, 3H, $C\underline{H}_3$).

*Ethyl 6-(ethylcarbamoyl)picolinate (**2**).* Ethylamine hydrochloride (0.409 mg, 5.02 mmol, 1.0 equiv.), EDC.HCl (1.95 g, 12.55 mol, 2.5 equiv.), HOBt.H_2O (1.70 g, 12.55 mmol, 2.5 equiv.) and DIPEA (3.10 mL, 17.57 mmol, 3.5 equiv.) were dissolved in anhydrous DMF (50 mL). 6-(methoxycarbonyl)picolinic acid **1** (1.00 g, 5.52 mmol, 1.1 equiv.) was dissolved in anhydrous DMF (20 mL) and added dropwise to the reaction mixture. The reaction was stirred at ambient temperature for 36 hours. The solvent was removed in vacuo. The compound was partitioned between H_2O (50 mL) and EtOAc (50 mL). The aqueous phase was further extracted with EtOAc (3 × 50 mL). The organic fractions were combined and dried over Na_2SO_4. The solvent was removed *in vacuo* and the residue was purified by column chromatography (SiO_2; MeOH/DCM; 0:100 to 2:98) to obtain compound **2** as a beige solid (586 mg, 2.81 mmol, 56%). ^{1}H NMR (500 MHz, 298 K, $CDCl_3$): δ 8.31 (dd, 1H, *J* = 1.2 Hz, *J* = 8 Hz, Py$\underline{H}$), 8.13 (dd, 1H, *J* = 1.3 Hz, *J* = 7.5 Hz, Py$\underline{H}$), 8.06 (br. s, 1H, N$\underline{H}$), 7.93 (t, 1H, *J* = 8 Hz, Py$\underline{H}$), 3.93 (s, 3H, O-C$\underline{H}_3$), 3.49-3.43 (m, 2H, NHC$\underline{H}_2$CH$_3$), 1.21 (t, 3H, *J* = 7.25 Hz, NHCH$_2$C$\underline{H}_3$). ^{13}C NMR (126 MHz, 298 K, $CDCl_3$): δ 164.9 (C$\underline{O}$CH$_3$), 163.2 (C$\underline{O}$NH), 150.4 (C-Py), 146.4 (C- Py), 138.5 (CH-Py), 127.1 (CH-Py), 125.3 (CH-Py), 52.8 (O$\underline{C}$H$_3$), 34.4 (NH$\underline{C}$H$_2$CH$_3$), 14.8 (NHCH$_2\underline{C}$H$_3$). ESI-MS: m/z calcd. for $[C_{10}H_{12}N_2O_3Na]^+$: 231.08; found 231.07. Anal. Calcd for $C_{10}H_{12}N_2O_3$ (208,21 g.mol^{-1}): C, 57.68; H, 5.81; N, 13.45. Found: C, 57.48; H, 5.80; N, 13.14.

*N-Ethyl-6-(hydroxymethyl)picolinamide (**3**).* Ethyl 6-(ethylcarbamoyl)picolinate **2** (571 mg, 2.74 mmol, 1.0 equiv.) was dissolved in CH_2Cl_2/MeOH (70 mL; 1:1). $NaBH_4$ (1.04 g, 27.4 mmol, 10.0 equiv.) was added portion wise over 20 minutes and the reaction was stirred during 1h. The reaction was acidified to pH = 5 with 1M $HCl_{(aq)}$ and then was basified to pH = 8 by the addition of $NaHCO_3$. The reaction was extracted with CH_2Cl_2 (10 × 50 mL) and the combined organic layers were dried over Na_2SO_4. The solvent was removed *in vacuo* to give compound **3** as a colorless oil (493 mg, 2.66 mmol, 97%). ^{1}H NMR (500 MHz, 298 K, MeOD): δ 7.95 (dd, 1H, *J* = 1.2 Hz, *J* = 7.75 Hz, Py$\underline{H}$), 7.90 (t, 1H, *J* = 7.6 Hz, Py$\underline{H}$), 7.59-7.57 (m, 1H, py$\underline{H}$), 4.75 (s, 2H, C$\underline{H}_2$OH), 3.46-3.42 (m, 2H, NHC$\underline{H}_2$CH$_3$), 1.23 (t, 3H, *J* = 7.5 Hz, NHCH$_2$C$\underline{H}_3$).). ^{13}C NMR (126 MHz, 298 K, MeOD): δ 166.4 (C$\underline{O}$-NH), 161.4 (C-Py), 150.3 (C-Py), 139.2 (CH-Py), 124.3 (CH-Py), 121.4 (CH-Py), 65.5 (CH$_2$-OH), 35.3 (NH$\underline{C}$H$_2$CH$_3$), 14.9 (NHCH$_2\underline{C}$H$_3$). ESI-MS: m/z calcd. for $[C_9H_{11}DN_2O_2Na]^+$: 204.09; found 204.09. Anal. Calcd for $C_9H_{12}N_2O_2$ (185.61 g.mol^{-1}): C, 58.24; H, 6.84; N, 15.09. Found: C, 58.44; H, 6.76; N, 14.82.

*6-(Chloromethyl)-N-ethylpicolinamide (**4**).* *N*-ethyl-6-(hydroxymethyl)picolinamide **3** (486 mg, 2.70 mmol, 1.0 equiv.) was dissolved in CH_2Cl_2 (20 mL) under Ar. $SOCl_2$ (274 µL, 3.78 mmol, 1.4 equiv.) was added dropwise and the reaction was stirred for 18 hours. The solvent was removed *in vacuo* and the residue was coevaporated with $CHCl_3$ (2 × 10 mL) to give compound **4** as a colourless oil (534 mg, 2.69 mmol, >99%). ^{1}H NMR (500 MHz, 298 K, $CDCl_3$): δ 8.13 (dd, 1 H, *J* = 1 Hz, *J* = 7.5 Hz, Py$\underline{H}$), 8.00 (brs, 1H, N$\underline{H}$), 7.86 (t, 1H, *J* = 7.5 Hz, Py$\underline{H}$), 7.58 (dd, 1H, *J* = 1.5 Hz, *J* = 7.5 Hz, Py$\underline{H}$), 4.66 (s, 2H, C$\underline{H}_2$-Cl), 3.53-3.47 (m, 2H, C$\underline{H}_2$-CH$_3$), 1.26 (t, 3H, *J* = 7 Hz, CH$_2$-C$\underline{H}_3$). ^{13}C NMR (126 MHz, 298 K, $CDCl_3$): δ 163.6 (CO), 155.2 (C-Py), 149.7 (C-Py), 138.5 (CH-Py), 125.2 (CH-Py), 121.6 (CH-Py), 46.1 (C$\underline{H}_2$-Cl), 34.3 (C$\underline{H}_2$-CH$_3$), 14.9 (CH$_2$-C$\underline{H}_3$). ESI-MS: m/z calcd. for $[C_9H_{11}ClN_2ONa]^+$: 221.06; found 221.05. Anal. Calcd for $C_9H_{11}ClN_2O$ (198.65 g mol^{-1}): C, 54.42; H, 5.58; N, 14.10. Found: C, 54.25; H, 5.49; N, 14.02.

*Macrocycle (**7**).* A Schlenk flask was charged with K_2CO_3 (300 mg, 2.17 mmol) and dried under dynamic vacuum with heating and backfilled with Ar. Tacn **5** (280 mg, 2.17 mmol) and diethyl (6-(chloromethyl) pyridine-2-yl) phosphonate **6** (1.14 g, 4.34 mmol) were added under argon and after 1h under vacuum, were dissolved in CH_3CN (5 mL). The reaction mixture was stirred during 1 day at 60°C. The remaining K_2CO_3 was removed by filtration, and the solvent was removed under reduced pressure. Purification of the crude product was performed by column chromatography over alumina (CH_2Cl_2/MeOH gradient from 100:00 to 95:5), yielding compound **7** (550 mg, 43%) as yellow oil. ^{1}H NMR (500 MHz, 298 K, $CDCl_3$): δ 7.68-7.60 (m, 4H, Py$\underline{H}$), 7.32 (td, 2H, *J* = 7.7 Hz, *J* = 1.9 Hz, Py$\underline{H}$), 4.14-4.04 (m, 8H, O-C$\underline{H}_2$-CH$_3$), 3.87 (s, 4H, Py-C$\underline{H}_2$), 3.27 (t, 4H, *J* = 6 Hz, TACN-C$\underline{H}_2$), 2.99 (t, 4H, *J* = 6 Hz, TACN-C$\underline{H}_2$), 2.58 (s, 4H, TACN-C$\underline{H}_2$), 1.20 (t, 12H, *J* = 7 Hz, O-CH$_2$-C$\underline{H}_3$). ^{13}C NMR (126 MHz, 298 K, $CDCl_3$): δ 159.7 (d, *J* = 21.3 Hz), 151.5 (d, *J* = 226.3 Hz), 136.9 (d, *J* = 11.3 Hz), 126.6 (d, *J* = 23.8 Hz), 125.6 (d, *J* = 3.8 Hz), 63.1 (d, *J* = 6.3 Hz), 60.9, 52.6, 50.0, 42.3, 16.5 (d, *J* = 6.3 Hz). ^{31}P NMR spectrum (162 MHz, 298 K, $CDCl_3$) : δ 10.74. ESI-MS: m/z calcd. for $[C_{26}H_{44}N_5O_6P_2]^+$: 584.27; found 584.28. Anal. Calcd for $C_{26}H_{44}N_5O_6P_2{\cdot}CH_2Cl_2$ (670.54 g mol^{-1}): C, 48.43; H, 6.92; N, 10.46. Found: C, 48.50; H, 7.25; N, 10.82.

*Compound **8**.* A Schlenk flask was charged with K_2CO_3 (63 mg, 0.456 mmol) and dried under dynamic vacuum with heating and backfilled with Ar. Macrocycle **7** (133 mg, 0.228 mmol)

and 6-(chloromethyl)-*N*-ethylpicolinamide **4** (50 mg, 0.252 mmol) were dissolved in anhydrous MeCN (3 mL) and added in the Schlenk flask. The reaction was heated at 40 °C under Ar for two days. The reaction was cooled down to room temperature and the solvent removed in vacuo. Purification of the crude product was performed by column chromatography over Alox (DCM/MeOH gradient from 100:0 to 95:5), yielding compound **8** (147 mg, 87%) as a yellow oil. ^{1}H NMR (500 MHz, 298 K, $CDCl_3$): δ 7.98 (d, 1H, *J* = 8 Hz, PyH), 7.74-7.66 (m, 5H, PyH), 7.57 (d, 2H, *J* = 7.5 Hz, PyH), 7.50 (d, 1H, *J* = 7.5 Hz, PyH), 4.21-4.06 (m, 8H, O-C$\underline{H_2}$-CH_3), 3.86 (s, 4H, Py-C$\underline{H_2}$), 3.81 (brs, 2H, Py-C$\underline{H_2}$), 3.47-3.35 (m, 2H, NH-C$\underline{H_2}$-CH_3), 3.00-2.54 (brs, 12H, 1.24 (t, 12H, *J* = 7 Hz, O-CH_2-C$\underline{H_3}$), 1.18-1.13 (m, 3H, NH-CH_2-C$\underline{H_3}$). ^{13}C NMR (126 MHz, 298 K, $CDCl_3$): δ 164.2, 152.0, 150.2, 137.7, 163.3 (d, *J* = 12.5 Hz), 126.3 (d, *J* = 24.4 Hz), 125.5, 64.2, 62.9 (d, *J* = 5.7 Hz), 55.8, 34.8, 16.3 (d, *J* = 6.3 Hz), 14.9. ^{31}P NMR spectrum (162 MHz, 298 K, $CDCl_3$) : δ 11.07. ESI-MS: m/z calcd. for $[C_{35}H_{54}N_7O_7P_2]^+$: 746.35; found 746.35. Anal. Calcd for $C_{35}H_{53}N_7O_7P_2{\cdot}CH_2Cl_2$ (830.72 g mol^{-1}): C, 52.05; H, 6.67; N, 11.80; Found: C, 52.29; H, 6.88; N, 11.81.

*Ligand **L1**.* To a Schlenk tube containing compound **8** (107 mg, 0.143 mmol), dissolved in anhydrous CH_2Cl_2 (3 mL) under argon, was added dropwise TMSBr (188 µL, 1.43 mmol). The reaction mixture was stirred during 18h. The solvent was removed in *vacuo* and the residue was taken up in MeOH. The solvent was removed under reduced pressure. The same procedure was then repeated with H_2O. Purification of the crude product was performed by column chromatography over C_{18} (H_2O/CH_3CN/TFA 0.1% gradient from 95:5 to 0:100), yielding ligand **L1**·$2C_2HF_3O_2{\cdot}2H_2O$ as a brown solid (79 mg, 87%). ^{1}H NMR (500 MHz, 298 K, D_2O): δ 8.35-8.31 (m, 2H), 8.05-7.96 (m, 5H), 7.82 (d, 2H, *J* = 7.5 Hz), 7.68 (d, 1H, *J* = 7.5 Hz), 4.63 (s, 2H), 4.39 (s, 4H), 3.68 (t, br, 4H), 3.31 (q, 2H, *J* = 7.5 Hz, *J* = 14.7 Hz), 3.23 (t, br, 4H), 3.03 (s, 4H), 1.06 (t, 3H, *J* = 7.3 Hz). ^{13}C NMR (126 MHz, 298 K, D_2O) 165.9, 135.5, 152.2 (t, *J* = 10.7 Hz), 149.8, 149.2, 144.9, 140.9, 128.1, 128.0, 127.5, 123.0, 59.7, 56.7, 51.5, 50.3, 48.0, 34.7, 13.6. ESI-MS: m/z calcd. for $[C_{27}H_{37}N_7O_7P_2K]^+$: 672.22 found; 672.18. Anal. Calcd for $C_{27}H_{37}N_7O_7P_2{\cdot}2C_2HF_3O_2{\cdot}2H_2O$ (897.65 g mol^{-1}): C, 41.48; H, 4.83; N, 10.92. Found: C, 41.44; H, 4.75; N, 10.96.

*Complex [Eu**L1**]TFA.* **L1**·2TFA·$2H_2O$ (27.0 mg, 30.1 µmol) was dissolved in D_2O (1.5 mL) and the solution was basified with a solution of NaOD in D_2O to pD = 7. A solution of $EuCl_3.6H_2O$ in D_2O (ca. 0.6 equiv., 0.05 M) was added and the pD equilibrated to 7. The reaction progress was monitored by ^{1}H NMR to calculate remaining free ligand. Additional $EuCl_3.6H_2O$ solution was added to give 1.0 equiv. in total and the reaction mixture was basified to pD =7. The solvent was removed *in vacuo* and the crude was purified by reversed phase chromatography (C_{18}, H_2O/CH_3CN/TFA 0.1% 95:5 to 0:100) to give [Eu**L1**]TFA as a white solid (16.0 mg, 20.4 µmol, 67%). ^{1}H NMR (400 MHz, 298 K, D_2O, pD 6.9) : δ 10.74 (s, 1H), 10.43 (s, 1H), 9.36 (d, *J* = 7.8 Hz, 1H), 9.14 (s, 1H), 8.84 (t, *J* = 7.8 Hz, 1H), 8.59 (s, 1H), 8.36 (d, *J* = 7.9 Hz, 1H), 8.13 (t, *J* = 6.1 Hz, 1H), 8.00 (s, 1H), 7.66 (t, *J* = 8.0 Hz, 1H), 6.77 (s, 1H), 6.54 (s, 1H), 6.35 (d, *J* = 7.9 Hz, 1H), 6.28 (t, *J* = 7.6 Hz, 1H), 3.68 (s, 1H), 3.49 (s, 1H), 2.85 (d, *J* = 7.2 Hz, 1H), -2.94 (s, 1H), -3.61 (s, 1H), -4.15 (s, 1H), -4.62 (s, 1H), -7.06 (d, *J* = 14.3 Hz, 1H), -12.22 (s, 1H), -13.40 (s, 1H), -14.13 (d, 1H, *J* = 12.0 Hz). ^{31}P NMR spectrum (162 MHz, 298 K, D_2O, pD 6.9) : δ 3.31, -16.12. ESI-MS: m/z calcd. for $[C_{27}H_{35}EuN_7O_7P_2]^+$: 784.13, found 784.13. Anal. Calcd for $[C_{27}H_{37}EuN_7O_7P_2]{\cdot}(C_2F_3O_2){\cdot}2(C_2HF_3O_2){\cdot}2(H_2O)$ (1162.63 g.mol^{-1}): C, 34.09; H, 3.73 N, 8.43. Found: C, 34.26; H, 3.43; N, 8.36.

*Complex [Tb**L1**]TFA.* **L1**·2TFA·$2H_2O$. (25.0 mg, 27.9 µmol) was dissolved in D_2O (1.5 mL) and the solution was basified with a solution of NaOD in D_2O to pD = 7. A solution of $TbCl_3.6H_2O$ in D_2O (0.04 M) was added by increasing aliquots (ca. 0.1 equiv. to 1 equiv.). The pD was equilibrated to 7 after each aliquot and the reaction progress was monitored to calculate remaining free ligand. The solvent was removed *in vacuo* and the crude was purified by reversed phase chromatography (C_{18}, H_2O/CH_3CN/TFA 0.1% 95:5 to 0:100) to give [Tb**L1**]TFA as a white solid (13.0 mg, 16.4 µmol, 59%). ^{1}H NMR (400 MHz, 298 K, D_2O): δ 109.69 (s, 1H), 102.22 (s, 1H), 97.54 (s, 1H), 18.01 (s, 1H), 13.76 (s, 1H), 7.12 (s, 1H), -4.62 (s, 1H), -7.92 (s, 1H), -13.91 (s, 1H), -20.97 (s, 1H), -26.70 (s, 1H), -30.00 (s,1H), -40.82 (s, 1H), -51.71 (s, 1H), -71.45 (s, 1H), -75.82 (s, 1H), -94.25 (s, 1H), -141.54 (s, 1H). ^{31}P NMR spectrum (162 MHz, 298 K, D_2O) : δ -3.10. ESI-MS m/z calcd. for $[C_{27}H_{35}TbN_7O_7P_2]^+$: 790.13, found 790.13. Anal. Calcd for $[C_{27}H_{37}N_7O_7P_2Tb]{\cdot}(C_2F_3O_2){\cdot}(C_2HF_3O_2){\cdot}2(H_2O)$ (1169.59 g.mol^{-1}): C, 33.89; H, 3.71; N, 8.38. Found: C, 34.01; H, 3.51; N, 8.25.

*Complex [Yb**L1**]TFA.* **L1**·2TFA·$2H_2O$ (45.0 mg, 50.1 µmol) was dissolved in D_2O (1.5 mL) and the solution was basified with a solution of NaOD in D_2O to pD = 7. A solution of $YbCl_3.6H_2O$ in D_2O (0.072 M) was added by increasing aliquots (ca. 0.1 equiv. to 1 equiv.). The pD was equilibrated to 7 after each aliquot and the reaction progress was monitored to calculate remaining free ligand. The solvent was removed *in vacuo* and the crude was purified by reversed phase chromatography (C_{18}, H_2O/CH_3CN/TFA 0.1% 95:5 to 0:100) to give [Yb**L1**]TFA as a white solid (20.0 mg, 24.8 µmol, 50%). ^{1}H NMR (400 MHz, 298 K, D_2O) : δ 88.78 (s, 1H), 37.15 (s, 1H), 36.73 (s, 1H), 33.87 (s, 1H), 26.73 (s, 1H), 23.80 (s, 1H), 21.40 (s, 1H), 18.44 (s, 1H), 17.69 (s, 4H), 17.44 (s, 1H), 17.17 (s, 1H), 14.58 (s, 1H), 12.97 (s, 1H), 11.15 (s, 1H), 8.44 (s, 1H), 7.56 (s, 1H), 3.14 (s, 1H), 2.36 (s, 1H), 1.07 (s, 1H), -2.83 (s, 1H), -6.52 (s, 1H), -12.20 (s, 2H), -14.00 (s, 1H), -22.90 (s, 1H), -28.05 (s, 1H), -29.90 (s, 1H), -37.46 (s, 1H), -54.36 (s, 1H). ^{31}P NMR spectrum (162 MHz, 298 K, D_2O): δ 0.13, -54.13. ESI-MS m/z calcd. for $[C_{27}H_{35}YbN_7O_7P_2]^+$: 805.15, found 805.15. Anal. Calcd for $[C_{27}H_{37}N_7O_7P_2Yb]$. $(C_2F_3O_2){\cdot}3(C_2HF_3O_2){\cdot}6(H_2O)$ (1369.81 g.mol^{-1}): C, 30.69; H, 3.83; N, 7.16. Found: C, 30.73; H, 3.14; N, 7.44.

*Complex [Lu**L1**]TFA.* **L1**·2TFA·$2H_2O$ (22 mg, 24.2 µmol) was dissolved in D_2O (1.5 mL) and the solution was basified with a solution of NaOD in D_2O to pD = 7. A solution of $LuCl_3.6H_2O$ in D_2O (0.072 M) was added by increasing aliquots (ca. 0.1 equiv. to 1 equiv.). The pD was equilibrated to 7 after each

aliquot and the reaction progress was monitored to calculate remaining free ligand. The solvent was removed *in vacuo* and the crude was purified by reversed phase chromatography (C_{18}, H_2O/CH_3CN 95:5 to 0:100) to give [Lu**L1**]TFA as a white solid (19.0 mg, 23.6 µmol, 92%). ^{1}H NMR (400 MHz, 298 K, D_2O): δ 8.18 (t, *J* = 8.1 Hz, 1H), 8.06-7.96 (m, 3H), 7.80-7.74 (m, 3H), 7.54 (dd, *J* = 7.8 Hz, *J* = 25.6 Hz), 9.00 (dd, *J* = 14.0 Hz, *J* = 7.3 Hz, 2H), 4.07-3.99 (m, 3H), 3.75 (d, *J* = 15.2 Hz, 1H), 2.95-2.60 (m, 7H), 2.59-2.48 (m, 2H), 2.30 (td, *J* = 12.7 Hz, *J* = 5.4 Hz, 1H), 1.95 (td, *J* = 12.7 Hz, J = 5.4 Hz, 1H), 0.74 (t, *J* = 7.3 Hz, 3H). ^{31}P NMR spectrum (162 MHz, 298 K, D_2O): δ 13.09, 12.26. ESI-MS m/z calcd. for $[C_{27}H_{35}LuN_7O_7P_2]^+$ 806.15, found 806.15. Anal. Calcd for $[C_{27}H_{37}LuN_7O_7P_2](CF_3CO_2)_3{\cdot}2(H_2O)$ (1183.62 g.mol^{-1}): C, 33.49; H, 3.49; N, 8.28. Found: C, 33.95; H, 3.57; N, 8.28

*Compound **12.*** To a solution of pyclen derivative **11** (379 mg, 1.36 mmol), K_2CO_3 (754 mg, 5.45 mmol, 4 equiv.) and NaI (419 mg, 2.79 mmol, 2.05 equiv.) in CH_3CN (31 mL) was added compound **6** (736 mg, 2.79 mmol, 2.05 equiv.). The reaction mixture was stirred at 40°C for 6 days. Salts were filtered off and the filtrate was evaporated to dryness. The residue was taken up in $CHCl_3$ and residual salts were filtered on cotton. The oily residue was then submitted to several precipitations (in MeOH/Et_2O and MeOH/CH_2Cl_2) and to a purification by column chromatography (Al_2O_3, eluent: CH_2Cl_2/MeOH 100/1 to 100/2) to give compound **12** (446 mg, 0.61 mmol, 44%) as a brown oil. ^{1}H-NMR (500 MHz, $CDCl_3$): δ 7.85 (m, 1H, ArH), 7.77 (m, 1H, ArH), 7.69 (m, 2H, ArH), 7.61 (t, *J* = 7.6 Hz, 1H, ArH), 7.58-7.50 (m, 1H, ArH), 7.45 (t, *J* = 8.4 Hz, 1H, ArH), 7.10 (d, *J* = 7.6 Hz, 1H, Ar pyclen), 7.04 (d, *J* = 7.7 Hz, 1H, Ar pyclen), 4.20-3.95 (m, 14H, H24, CH_2 pyclen), 3.80-3.60 (m, 8H, H17, CH_2 pyclen), 3.06 (m, 1H, CH_2 pyclen), 2.85-2.81 (m, 1H, CH_2 pyclen), 2.60 (d, *J* = 14.6 Hz, 1H, CH_2 pyclen), 2.55-2.49 (m, 1H, CH_2 pyclen), 2.36-2.31 (m, 2H, CH_2 pyclen), 1.75-1.69 (m, 1H, CH_2 pyclen), 1.29 (m, 9H, H25), 1.19 (t, *J* = 7.1 Hz, 3H, H25). ^{31}P-NMR (202 MHz, $CDCl_3$): δ 12.00, 11.88. ^{13}C-NMR (126 MHz, $CDCl_3$): δ 173.4 (C16), 158.6, 158.1 (C1 and C11), 158.5 (d, *J* = 20 Hz, C19 or C19'), 158.1 (d, *J* = 17.5 Hz, C19 or C19'), 151.2 (d, *J* = 224 Hz, C23 or C23'), 150.9 (d, *J* = 226 Hz, C23 or C23'), 138.1 (C13), 137.5 (d, *J* = 12.5 Hz, C21 or C21'), 137.1 (d, *J* = 11.3 Hz, C21 or C21'), 127.0 (d, *J* = 2.5 Hz, C20 or C20'), 126.7 (d, *J* = 2.5 Hz, C20 or C20'), 126.0 (d, *J* = 23.7 Hz, C22 and C22'), 121.5 (C12), 120.9 (C14), 62.9 (m, C24), 62.2, 61.6, 61.1, 59.7, 57.4, 56.4, 54.1, 52.4, 52.1 (C2, C4, C5, C7, C8, C10, C15, C18, C18'), 51.9 (C17), 16.3 (d, *J* = 5 Hz, C25). ESI-HR-MS (positive) *m/z* calcd. for $[C_{34}H_{51}N_6O_8P_2]^+$: 733.3238, found: 733.3237, $[M+H]^+$; calcd. for $[C_{34}H_{50}N_6NaO_8P_2]^+$: 755.3057, found: 755.3049, $[M+Na]^+$; calcd. for $[C_{34}H_{52}N_6O_8P_2]^{2+}$: 367.1655, found: 367.1662, $[M+2H]^{2+}$.

*Compound **13.*** To a solution of compound **12** (62 mg, 85 µmol) in CH_2Cl_2 (3.5 mL) was added dropwise TMSBr (223 µL, 1.69 mmol, 20 equiv.) and the reaction mixture was stirred at room temperature for 24h. $CHCl_3$ was then added to the reaction mixture until formation of a precipitate. The precipitate was filtered on cotton and rinsed with $CHCl_3$. The solid on cotton was then dissolved in H_2O and evaporated to dryness. The residue was submitted to a precipitation in water/acetone to give quantitively compound **13** as a yellow oil which was used in the next step without further purification. ESI-HR-MS (negative) *m/z*; calcd. for $[C_{26}H_{32}N_6NaO_8P_2]^-$: 641.1660, found: 641.1656, $[M-2H+Na]^-$; calcd. for $[C_{26}H_{33}N_6O_8P_2]^-$: 619.1840, found: 619.1830, $[M-H]^-$.

*Ligand **L2**.* A solution of compound **13** (54 mg, 87 µmol) in 3 M HCl (2 mL) was stirred at 80°C for 20h. Acetone was added in large excess until formation of an oil on the wall of the flask. The solvents were poured off and the residual oil on the flask was rinsed with acetone to give compound **L2** (39 mg, 54 µmol, 62%) as a brown oil. Sometimes compound **L2** needed a purification by flash chromatography (column C_{18}, eluent: H_2O/ACN 100/0 à 0/100) but the final yield decreased dramatically from 27 to 62%. The ligand was obtained as a trichlorohydrate salt **L2**·3HCl. ^{1}H-NMR (500 MHz, D_2O, 298 K): δ 8.11 (m, 1H, H21'), 8.05 (m, 1H, H21), 8.02-7.94 (m, 4H, H13, H20, H22, H22'), 7.63 (d, *J* = 7.9 Hz, 1H, H20'), 7.54 (d, *J* = 7.8 Hz, 1H, H12), 7.41 (d, *J* = 7.9 Hz, 1H, H14), 4.86 (s, 2H, H10), 4.56 (s, 2H, H2), 4.49 (s, 2H, H18'), 4.36 (s, 2H, H18), 4.23 (s, 2H, H15), 3.87 (s, 2H, H8), 3.53 (s, 2H, H4), 3.25 (s, 2H, H5), 3.14 (s, 2H, H7). ^{31}P-NMR (202 MHz, D_2O): δ 5.32, 0.60. ^{13}C-NMR (126 MHz, D_2O): δ 173.2 (C16), 157.4 (d, *J* = 202 Hz, C23 or C23'), 155.9 (d, *J* = 183 Hz, C23 or C23'), 155.3 (d, *J* = 11.4 Hz, C19), 153.2 (C1), 152.9 (C11), 152.6 (d, *J* = 16.9 Hz, C19), 147.3 (C13), 144.0 (C21'), 131.2 (d, *J* = 13.9 Hz, C22 or C22'), 130.9 (C20), 130.3 (d, *J* = 19.8 Hz, C22 or C22'), 129.7 (C20'), 126.6 (C12 and C14), 62.5 (C10), 60.4 (C15), 60.1 (C2), 59.4 (C18'), 58.2 (C18), 56.9 (C8), 54.2 (C4), 52.8 (C5), 52.7 (C7). ESI-HR-MS (negative) *m/z*; calcd. for $[C_{25}H_{30}N_6NaO_8P_2]^-$: 627.1503, found: 627.1496, $[M-2H+Na]^-$; calcd. for $[C_{25}H_{31}N_6O_8P_2]^-$: 605.1684, found: 605.1678, $[M-H]^-$; calcd. for $[C_{25}H_{29}CaN_6O_8P_2]^-$: 643.1153, found: 643.1146, $[M-3H+Ca]^-$.

*Complex [Lu**L2**].* Ligand **L2**·3HCl (12 mg, 17 µmol) was dissolved in D_2O (200 µL) and the pD was adjusted to 6.8 with 0.1 M NaOD before addition of $LuCl_3.6H_2O$ (201 µL of a 0.1 M solution in D_2O, 20 µmol, 1.2 equiv.). The pD was adjusted again to 6.8 with 0.1 M NaOD and the reaction mixture was stirred at 60°C for 15h. The precipitate was filtered on a pad of cotton and washed with D_2O. The filtrate was lyophilized to dryness to give [Lu**L2**] (13 mg, 17 µmol, 100%) as a white powder. ^{1}H-NMR (500 MHz, D_2O, 298 K): δ 8.05-8.02 (m, 1H, H21), 7.92-7.90 (m, 1H, H21'), 7.84 (t, *J* = 7.7 Hz, 1H, H13), 7.79-7.77 (m, 1H, H22), 7.60-7.56 (m, 2H, H20, H22'), 7.43 (d, *J* = 7.5 Hz, 1H, H20'), 7.40 (t, *J* = 6.8 Hz, 1H, H12), 7.13 (d, *J* = 7.8 Hz, 1H, H14), 5.19 (dd, *J* = 15.2, 1.0 Hz, 1H, H10a), 4.57 (d, *J* = 14.8 Hz, 1H, H18), 4.18-4.05 (m, 4H, H2a, H10b, H15a, H18'a), 4.00-3.94 (m, 2H, H2b, H18'b), 3.70 (d, *J* = 15.3 Hz, 1H, H18b), 3.45 (d, *J* = 15.6 Hz, 1H, H15a), 3.19-3.18 (m, 1H, H8a), 2.95 (d, *J* = 15.3 Hz, 1H, H5a), 2.87 (d, *J* = 15 Hz, 1H, H8b), 2.59-2.56 (m, 3H, H4a, H5b, H7a), 2.20-2.14 (m, 1H, H4b), 1.63-1.56 (m, 1H, H7b). ^{31}P-NMR (202 MHz, D_2O): δ 13.07, 11.09. ^{13}C-NMR (126 MHz, D_2O): δ 184.4 (C16), 162.1 (C1), 162.0 (C11), 163.9 (d, *J* = 122 Hz, C23 or C23'), 161.5 (d, *J* = 203 Hz, C23 or C23'), 159.6 (d, *J* = 16.2 Hz, C19), 158.2 (d, *J* = 15.3 Hz, C19'), 142.9 (C13), 142.5 (d, *J* = 9.1 Hz, C21), 141.4 (d,

J = 9.5 Hz, C21'), 128.4 (d, *J* = 18.4 Hz, C22), 127.3 (d, *J* = 19.4 Hz, C22'), 126.6 (C20'), 126.0 (C20), 123.6 (C12), 122.5 (C14), 67.2 (C2), 67.1 (C10), 66.8 (C15), 65.2 (C18), 64.7 (C5), 64.6 (C18'), 61.4 (C4), 61.1 (C7), 59.7 (C8). ESI-HR-MS (positive) *m/z* calcd. for $[C_{25}H_{30}LuN_6O_8P_2]^+$: 779.1002, found: 779.1009, $[M+H]^+$; calcd. for $[C_{25}H_{29}LuN_6NaO_8P_2]^+$: 801.0822, found: 801.0827, $[M+Na]^+$; calcd. for $[C_{25}H_{28}LuN_6Na_2O_8P_2]^+$: 823.0641, found: 823.0649, $[M-H+2Na]^+$; calcd. for $[C_{25}H_{30}LuN_6NaO_8P_2]^{2+}$: 401.0447, found: 401.046, $[M+H+Na]^{2+}$; calcd. for $[C_{25}H_{31}LuN_6O_8P_2]^{2+}$: 390.0537, found: 390.0551, $[M+2H]^{2+}$.

*Complex [Eu**L2**].* Ligand **L2**·3HCl (38 mg, 53 µmol) was dissolved in H_2O (2 mL) and the pH was adjusted to 6.0 with a 1 M KOH solution before addition of $EuCl_3.6H_2O$ (21 mg, 58 µmol, 1.1 equiv.). The pH was adjusted again to 6.6 with 0.1 M KOH and the reaction mixture was stirred at 60°C for 3 days. The reaction mixture was concentrated to 1 mL before addition of acetone in large excess. The precipitate was filtered over a pad of cotton and the solid on cotton was dissolved in H_2O. Water was evaporated and the residue was submitted to a dialysis process to remove salts in excess. After lyophilization, compound [Eu**L2**] (37 mg, 49 µmol, 95%) was obtained as a white powder. ESI-HR-MS (positive) *m/z* calcd. for $[C_{25}H_{30}EuN_6O_8P_2]^+$: 757.0807, found: 757.0811, $[M+H]^+$; calcd. for $[C_{25}H_{29}EuN_6KO_8P_2]^+$: 795.0365, found: 795.0363, $[M+K]^+$; calcd. for $[C_{25}H_{33}EuN_7O_8P_2]^+$: 774.1073, found: 757.0811, $[M+NH_4]^+$; calcd. for $[C_{25}H_{31}EuN_6O_8P_2]^{2+}$: 379.0439, found: 379.0453, $[M+2H]^{2+}$.

*Complex [Yb**L2**].* Ligand **L2**·3HCl (40 mg, 56 µmol) was dissolved in H_2O (2 mL) and the pH was adjusted to 6.3 with a 1 M KOH solution before addition of $YbCl_3.6H_2O$ (24 mg, 62 µmol, 1.1 equiv.). The pH was adjusted again to 6.8 with 0.1M KOH and the reaction mixture was stirred at 60°C for 20h. The reaction mixture was concentrated to 1 mL before addition of acetone in large excess. The precipitate was filtered over a pad of cotton and the solid was dissolved in H_2O. Water was evaporated and the residue was submitted to a dialysis process to remove salts in excess. After lyophilization, compound [Yb**L2**] (29 mg, 37 µmol, 67%) was obtained as a white powder. ESI-HR-MS (positive) *m/z* calcd. for $[C_{25}H_{30}YbN_6O_8P_2]^+$: 778.0983, found: 778.0979, $[M+H]^+$; calcd. for $[C_{25}H_{29}YbN_6KO_8P_2]^+$: 816.0542, found: 816.0534, $[M+K]^+$; calcd. for $[C_{25}H_{33}YbN_7O_8P_2]^+$: 795.1248, found: 795.1205, $[M+NH_4]^+$; calcd. for $[C_{25}H_{31}YbN_6O_8P_2]^{2+}$: 389.5528, found: 389.5529, $[M+2H]^{2+}$.

*Complex [Tb**L2**].* Ligand **L2**·3HCl (39 mg, 54 µmol) was dissolved in H_2O (4 mL) and the pH was adjusted to 6.3 with a 1 M KOH solution before addition of $TbCl_3.6H_2O$ (24 mg, 62 µmol, 1.1 equiv.). The pH was adjusted again to 6.3 with aqueous 0.1 M KOH and the reaction mixture was stirred at 60°C for 3 days. The reaction mixture was concentrated to 1 mL before addition of acetone in large excess. The precipitate was filtered over a pad of cotton and the solid was dissolved in H_2O. Water was evaporated and the residue was submitted to a dialysis process to remove salts in excess. After lyophilization, compound [Tb**L2**] (36 mg, 47 µmol, 87%) was obtained as a white powder. ESI-HR-MS (positive) *m/z* calcd. for $[C_{25}H_{30}TbN_6O_8P_2]^+$: 763.0848, found: 763.0858, $[M+H]^+$; calcd. for $[C_{25}H_{29}TbN_6KO_8P_2]^+$: 801.0407, found: 801.0407, $[M+K]^+$; calcd. for $[C_{25}H_{33}TbN_7O_8P_2]^+$: 780.1114, found: 780.1112, $[M+NH_4]^+$; calcd. for $[C_{25}H_{31}TbN_6O_8P_2]^{2+}$: 382.0461, found: 382.0472, $[M+2H]^{2+}$.

Spectroscopic measurements. Distilled water was purified by passing through a mixed bed of ion-exchanger (Bioblock Scientific R3–83002, M3-83006) and activated carbon (Bioblock Scientific ORC-83005). All the stock solutions were prepared by weighing solid products using an AG 245 Mettler Toledo analytical balance (precision 0.01 mg). Metal cation solutions were prepared from their metal chloride salt ($EuCl_3·6H_2O$, $TbCl_3·6H_2O$, $YbCl_3·6H_2O$, 99.9 %, Sigma-Aldrich), and their concentrations were determined by colorimetric titrations with EDTA (5.37×10^{-5} M, Merck, Titriplex III) according to standard procedures, using xylenol orange as indicator.[74]

UV/vis absorption spectra were recorded on a Specord spectrometer from Jena Analytics. Steady state emission spectra were recorded on an Edinburgh Instrument FLP920 spectrometer working with a continuous 450W Xe Lamp and a red sensitive R928 photomultiplier from Hamamatsu in Pelletier housing for visible detection (230 to 900 nm) or a Hamamatsu R5 509-72 photomultiplier for the Vis-NIR part. All spectra were corrected for the instrumental functions. For emission spectra upon UV excitation, a 330 nm cut-off filter was used to eliminate second order artefacts. Phosphorescence lifetimes were measured on the same instrument working in the Multi-Channel Spectroscopy (MCS) mode, using a Xenon flash lamp as the excitation source. For short µs lifetimes, the intensity decay was corrected for the lamp intensity decay profile using a scattering solution of Ludox in water. Luminescence quantum yields were measured according to conventional procedures,[75] with optically diluted solutions (optical density < 0.05), using $[Ru(bipy)_3Cl_2]$ in water (Φ = 0.04)[76] as reference for Eu, a bipyridine Tb complex, $[TbL(H_2O)]$ in water (Φ = 0.31)[77] as reference for Tb, and cardiogreen (IR125) in MeOH (Φ = 0.078) for Yb.[78] The errors are estimated to 10 % on the lifetimes and 15 % on the luminescence quantum yields. Hydrations numbers, q, were obtained using equation of Beeby *et al*.[67]

Computational details. Geometry optimizations of the [Yb**L1**] and [Lu**L2**] systems were carried out with density functional theory (DFT) using the Gaussian16 program[79] and the TPSSh[80] functional. The lanthanides were treated using the large-core approximation, which incorporates the 4f electrons of Yb and Lu in the core, while describing the outer 5s, 5p, 5d, and 6s electrons with a (7s6p5d)/[5s4p3d]-GTO valence basis set.[81] The 6-31G(d,p) basis set was used for all other atoms. The criteria for the convergence of the self-consistent field calculations and the size of the integration grid were set with the scf=tight and Integral=superfinegrid keywords. Bulk solvent effects (water) were incorporated with the integral equation formalism of the polarized continuum model (IEF-PCM).[82]

Molecular volumes were estimated using the volume=tight keyword.

Complete active space self-consisted field (CASSCF)[83] calculations were performed using the ORCA5[84, 85] program system (Program Version 5.0.3). Dynamic correlation was introduced with N-electron valence perturbation theory to second order (FIC-NEVPT2).[86, 87] Relativistic effects were incorporated with the second-order Douglas-Kroll-Hess (DKH2)[88, 89] approximation and a finite nucleus model.[90] The active space included the 13 Yb electrons distributed in the seven metal-based 4f orbitals [CAS(13,7)]. The integration grids were increased from the defaults using the AngularGrid 7 and IntAcc 5.0 options within the %method section. Bulk water solvent effects were introduced with the SMD model proposed by Truhlar.[91] Spin-orbit coupling effects were incorporated within the framework of quasi-degenerate perturbation theory (QDPT).[92, 93] For ligand atoms, we selected the DKH-def2-TZVPP basis set recontracted for DKH2 calculations by D. A. Pantazis taking the exponents from the def2-TZVPP basis set.[94] The Yb atom was described with the SARC2-DKH-QZVP[95] basis sets. The resolution of identity and chain of spheres (RIJCOSX)[96-98] approach accelerated the calculations with the aid of the SARC2-DKH-QZVP/JK[95] auxiliary basis set for Yb and the auxiliary basis sets generated with the Autoaux[99] procedure for all other atoms.

ACKNOWLEDGEMENTS

The authors acknowledge the Ministère de l'Enseignement Supérieur et de la Recherche and the Centre National de la Recherche Scientifique. The authors are also grateful to Agence National de la Recherche (LUCAS ANR-19-CE29-0014-01) for financial support.

ASSOCIATED CONTENT

Supporting Information. Analytical HPLC chromatograms, NMR spectra and HR-MS analysis of all compounds including the complexes, spectroscopic characterization, theorical calculations, etc. are given in the supporting information. This material is available free of charge via the Internet at http://pubs.acs.org.

AUTHOR INFORMATION

Corresponding Author

* Raphaël Tripier; orcid.org/0000-0001-9364-788X;
Email: raphael.tripier@univ-brest.fr
* Loïc J. Charbonnière ; orcid.org/0000-0003-0328-9842
Email: l.charbonn@unistra.fr

Author Contributions

The manuscript was written through contributions of all authors. All authors have given approval to the final version of the manuscript.

REFERENCES

1) Caravan, P., Ellison, J. J.; McMurry, T. J.; Lauffer, R. B. Gadolinium(III) Chelates as MRI Contrast Agents: Structure, Dynamics, and Applications. *Chem. Rev.* **1999**, *99*, 2293–2352.
2) Bottrill, M.; Kwok, L.; Long, N. J. Lanthanides in magnetic resonance imaging. *Chem. Soc. Rev.* **2006**, *35*, 557–571.
3) Sorace, L.; Benelli, C.; Gatteschi, D. Lanthanides in molecular magnetism: Old tools in a new field. *Chem. Soc. Rev.* **2011**, *40*, 3092-3104.
4) Bünzli, J.-C. G.; Piguet, C. Taking advantage of luminescent lanthanide ions. *Chem. Soc. Rev.* **2005**, 34, 1048-1077.
5) Hemmilä, I.; Laitala, V. Progress in lanthanides as luminescent probes. *J. Fluoresc.* **2005**, *15*, 529-542.
6) Eliseeva, S. V.; Bünzli, J.-C. G. Lanthanide luminescence for functional materials and bio-sciences. *Chem. Soc. Rev.* **2010**, *39*, 189-227.
7) Monteiro, J. H. S. K. Recent Advances in Luminescence Imaging of Biological Systems Using Lanthanide(III) Luminescent Complexes. *Molecules* **2020**, *109* (25), 2089-2123.
8) Hildebrandt, N.; Charbonnière, L. J.; Löhmannsröben, H.-G. Time-Resolved Analysis of a Highly Sensitive Förster Resonance Energy Transfer (FRET) Immunoassay Using Terbium Complexes as Donors and Quantum Dots as Acceptors. *J. Biomed. Biotech.* **2007**, *2007*, 1-6.
9) Sy, M.; Nonat, A.; Hildebrandt, N.; L. J. Charbonnière, L. J. Lanthanide-based luminescent biolabeling. *Chem. Comm.* **2016**, *52*, 5080-5095.
10) Zhang, X. Zhu, T.; Cheng, C. C. W.; Kwok, W.-M.; Tam, H.-L.; Hao, J.; Kwong, D.W. J.; Wong, W.-K.; Wong, K.-L. Water-Soluble Mitochondria-Specific Ytterbium Complex with Impressive NIR Emission. *J. Am. Chem.Soc.* **2011**, *133*, 20120-20122.
11) D'Aléo, A.; Bourdolle, A.; Brustlein, S.; Fauquier, T.; Grichine, A.; Duperray, A.; Baldeck, P. L.; Andraud, C.; Brasselet, S.; Maury, O. Ytterbium-based bioprobes for near-infrared two-photon scanning laser microscopy imaging. *Angew. Chem., Int. Ed.* **2012**, *51*, 6622-6625.
12) Bui, A. T.; Beyler, M.; Grichine, A.; Duperray, A.; Mulatier, J. C.; Guyot, Y.; Andraud, C.; Tripier, R.; Brasselet, S.; Maury, O. Near infrared two photon imaging using a bright cationic Yb(III) bioprobe spontaneously internalized into live cells. *Chem. Commun.* **2017**, *53*, 6005-6008.
13) Gavriluta, A.; Fix, T.; Nonat, A.; Slaoui, A.; Guillemoles, J.-F.; Charbonnière, L.J. «Tuning the chemical properties of europium complexes as downshifting agents for copper indium gallium selenide solar cells. *J. Mat. Chem. A.*, **2017**, 5, 14031-14040.
14) Souri, N.; Tian, P.; Platas-Iglesias, C.; Wong, K.-L.; Nonat, A.; Charbonnière, L. J. Upconverted Photosensitization of Tb Visible Emission by NIR Yb Excitation in Discrete Supramolecular Heteropolynuclear Complexes. *J. Am. Chem. Soc.* **2017**, *139*, 1456-1459.
15) Nonat, A.; Bahamyirou, S.; Lecointre, A.; Przybilla, F.; Mély, Y.; Platas-Iglesias, C.; Camerel, F.; Jeannin, O.; Charbonnière, L. J. Molecular Upconversion in Water in Heteropolynuclear Supramolecular Tb/Yb Assemblie. *J. Am. Chem. Soc.* **2019**, *141*, 1568−1576.

16) Weissman, S.I. Intramolecular Energy Transfer The Fluorescence of Complexes of Europium. *J. Chem. Phys.* **1942**, *10*, 214.
17) G. Mathis, H. Bazin, (2010). Stable Luminescent Chelates and Macrocyclic Compounds. In: Hänninen, P., Härmä, H. (eds) Lanthanide Luminescence. Springer Series on Fluorescence, vol 7. Springer, Berlin, Heidelberg.
18) Rodriguez-Rodriguez, A.; Esteban- Gómez, D.; Tripier, R.; Tircsó, G.; Garda, Z.; Toth, I.; de Blas, A.; Rodriguez-Blas, T.; Platas-Iglesias, C. Lanthanide(III) Complexes with a Reinforced Cyclam Ligand Show Unprecedented Kinetic Inertness. *J. Am. Chem. Soc.* **2014**, *136*, 17954−17957.
19) Rodriguez- Rodriguez, A.; Regueiro-Figueroa, M.; Esteban-Gómez, D.; Tripier, R.; Tircsó, G.; Kalman, F. K.; Benyei, C. A.; Toth, I.; de Blas, A.; Rodriguez-Blas, T.; Platas-Iglesias, C. Complexation of Ln^{3+} Ions with Cyclam Dipicolinates: A Small Bridge that Makes Huge Differences in Structure, Equilibrium, and Kinetic Properties. *Inorg. Chem.* **2016**, *55*, 2227−2239.
20) Parker, D. Luminescent lanthanide sensors for pH, pO_2 and selected anions. *Coord. Chem. Rev.* **2000**, *205*, 109-130.
21) Leonard, J.P., Gunnlaugsson, T. Luminescent Eu(III) and Tb(III) Complexes: Developing Lanthanide Luminescent-Based Devices. *J. Fluoresc.* **2005**, *15* (4), 585-595.
22) Montgomery, C. P.; Murray, B. S.; New, E. J.; Pal, R.; Parker, D. Cell-Penetrating Metal Complex Optical Probes: Targeted and Responsive Systems Based on Lanthanide Luminescence. *Acc. Chem. Res.* **2009**, *42*, 7, 925-937.
23) Liu, T.; Nonat, A.; Beyler, M.; Regueiro-Figueroa, M.; Nchimi Nono, K.; Jeannin, O.; Camerel, F.; Debaene, F.; Cianférani-Sanglier, S.; Tripier, R.; Platas-Iglesias C.; and Charbonnière, L.J. Supramolecular Luminescent Lanthanide Dimers for Fluoride Sequestering and Sensing. *Angew. Chem. Int. Ed*. **2014**, *53*, 7259-7263.
24) Regueiro-Figueroa, M.; Bensenane, B.; Ruscsák, E.; Esteban-Gómez, D.; Charbonnière, L. J.; Tircsó, G.; Tóth, I.; De Blas, A.; Rodríguez-Blas, T.; Platas-Iglesias, C. Lanthanide dota-like Complexes Containing a Picolinate Pendant: Structural Entry for the Design of Ln^{III}-Based Luminescent Probes. *Inorg. Chem.* **2011**, *50*, 4125-4141.
25) Rodríguez-Rodríguez, A.; Esteban-Gómez, D.; de Blas, A.; Rodríguez-Blas, T.; Fekete, M.; Botta, M.; Tripier, R.; Platas- Iglesias, C. Lanthanide(III) Complexes with Ligands Derived from a Cyclen Framework Containing Pyridinecarboxylate Pendants. The Effect of Steric Hindrance on the Hydration Number. *Inorg. Chem*. **2012**, *51* (4), 2509−2521.
26) Rodríguez-Rodríguez, A.; Garda, Z.; Ruscsák, E.; Esteban-Gómez, D.; de Blas, A.; Rodríguez-Blas, T.; Lima, L. M. P.; Beyler, M.; Tripier, R.; Tircsó, G.; Platas-Iglesias, C. Stable Mn^{2+}, Cu^{2+} and Ln^{3+} complexes with cyclen-based ligands functionalized with picolinate pendant arms. *Dalton Trans.* **2015**, *44* (11), 5017-5031.
27) Nonat, A.; Gateau, C.; Fries, P. H.; Mazzanti, M. Lanthanide Complexes of a Picolinate Ligand Derived from 1,4,7-Triazacyclononane with Potential Application in Magnetic Resonance Imaging and Time-Resolved Luminescence Imaging. *Chem Eur.-J.* **2006**, *12*,7133-7150.
28) Nakai, H.; Goto, T.; Kitagawa, K.; Nonaka, K.; Matsumoto, T.; Ogo, S. A highly luminescent and highly oxygen-sensitive Tb(III) complex with a tris-aryloxide functionalised 1,4,7-triazacyclononane ligand. *Chem. Commun.* **2014**, *50*, 15737-15739.
29) Bui, A.T.; Grichine, A.; Brasselet, S.; Duperray, A.; Andraud, C.; Maury, O. Unexpected Efficiency of a Luminescent Samarium(III) Complex for Combined Visible and Near-Infrared Biphotonic Microscopy. *Chem. Eur.-J.* **2015**, *21*, 17757-17761.
30) Neil, E. R.; Fox, M. A.; Pal, R.; Parker, D. Induced europium CPL for the selective signaling of phosphorylated amino-acids and O-phosphorylated hexapeptide. *Dalton Trans.* **2016**, *45*, 8355-8366.
31) Bui, A. T.; Grichine, A.; Duperray, A.; Lidon, P.; Riobé, F.; Andraud, C.; Maury, O. Terbium(III) Luminescent Complexes as Millisecond-Scale Viscosity Probes for Lifetime Imaging. *J. Am. Chem. Soc.* **2017**, *139* (23), 7693-7696.
32) Houlne, M. P.; Agent, T. S.; Kiefer, G. E.; McMillan, K.; Bornhop, D. J. Spectroscopic characterization and tissue imaging using site-selective polyazacyclic terbium(III) chelates. *Applied Spectro.* **1996**, *50* (10), 1221-1228.
33) Kiefer, G. E.; Woods, M. Solid State and Solution Dynamics of Pyridine Based Tetraaza-Macrocyclic Lanthanide Chelates Possessing Phosphonate Ligating Functionality (Ln-PCTMB): Effect on Relaxometry and Optical Properties. *Inorg. Chem.* **2009**, *48*, 11767-11778.
34) Le Fur, M.; Molnár, E.; Beyler, M.; Fougère, O.; Esteban-Gómez, D.; Rousseaux, O.; Tripier, R.; Tircsó, G.; Platas-Iglesias, C. Expanding the Family of Pyclen-Based Ligands Bearing Pendant Picolinate Arms for Lanthanide Complexation. *Inorg. Chem.* **2018**, *57*, 6932-6945.
35) Hamon, N.; Galland, M.; Le Fur, M.; Roux, A.; Duperray, A.; Grichine, A.; Andraud, C.; Le Guennic, B.; Beyler, M.; Maury, O.; Tripier, R. Combining a pyclen framework with conjugated antenna for the design of europium and samarium luminescent bioprobes. *Chem. Commun.* **2018**, *54*, 6173-6176.
36) Hamon, N.; Roux, A.; Beyler, M.; Mulatier, J.-C.; Andraud, C.; Nguyen, C.; Maynadier, M.; Bettache, N.; Duperray, A.; Grichine, A.; Brasselet, S.; Gary-Bobo, M.; Maury, O.; Tripier, R. Pyclen-Based Ln(III) Complexes as Highly Luminescent Bioprobes for In Vitro and In Vivo One- and Two-Photon Bioimaging Applications. *J. Am. Chem. Soc.* **2020**, *142*, 10184-10197.
37) Nizou, G.; Favaretto, C.; Borgna, F.; Grundler, P. V.; Saffon-Merceron, N.; Platas-Iglesias, C.; Fougère, O.; Rousseaux, O.; van der Meulen, N. P.; Müller, C.; Beyler, M.; Tripier, R. Expanding the Scope of Pyclen-Picolinate Lanthanide Chelates to Potential Theranostic Applications. *Inorg. Chem.* **2020**, *59*, 11736-11748.
38) Uzal-Varela, R.; Rodríguez-Rodríguez, A.; Wang, H.; Esteban-Gómez, D.; Brandariz, I.; Gale, E.M.; Caravan, P.; Platas-Iglesias, C. Prediction of Gd(III) complex thermodynamic stability. *Coord. Chem. Rev*. **2022**, *467*, 214606.

39) Lukes, I.; Kotek, J.; Vojtisek, P.; Hermann, P. Complexes of tetraazacycles bearing methylphosphinic/phosphonic acid pendant arms with copper(II), zinc(II) and lanthanides(III). A comparison with their acetic acid analogues. *Coord. Chem. Rev.* **2001**, *216–217*, 287-312.

40) Balogh, E.; Mato-Iglesias, M.; Platas-Iglesias, C.; Toth, E.; Djanashvili, K.; Peters, J. A.; de Blas, A.; Rodriguez-Blas, T. Pyridine and phosphonate containing acyclic ligands for stable lanthanide complexation. Extremely fast water exchange on the GdIII chelates. *Inorg. Chem.* **2006**, *45* (21), 8719-8728.

41) Knighton, R. C.; Soro, L. K.; Troadec, T.; Mazan, V.; Nonat, A. M.; Elhabiri, M.; Saffon-Merceron, N.; Djenad, S.; Tripier, R.; Charbonnière, L. J. Formation of Heteropolynuclear Lanthanide Complexes Using Macrocyclic Phosphonated Cyclam-Based Ligands. *Inorg. Chem.* **2020**, *59*, 10311-10327.

42) Abada, S.; Lecointre, A.; Elhabiri, M.; Platas-Iglesias, C.; Tallec, G.; Mazzanti, M.; Charbonnière L.J. Highly relaxing gadolinium-based MRI contrast agents responsive to Mg^{2+} sensing. *Chem. Commun.* **2012**, *48*, 4085-4087.

43) Elhabiri, M.; Abada, S.; Sy, M.; Nonat A.; Choquet, P.; Esteban-Gomez, D.; Cassino, C.; Platas-Iglesias, C.; Botta, M.; Charbonnière, L.J. Importance of Outer-Sphere and Aggregation Phenomena in the Relaxation Properties of Phosphonated Gadolinium Complexes with Potential Applications as MRI Contrast Agents. *Chem. Eur. J.* **2015**, *21*, 6535-6546.

44) Salaam, J.; Tabti, L.; Bahamyirou, S.; Lecointre, A.; Hernandez Alba, O.; Jeannin, O.; Camerel, F.; Cianférani, S.; Bentouhami, E.; Nonat, A. M.; Charbonnière, L. J. Formation of Mono- and Polynuclear Luminescent Lanthanide Complexes based on the Coordination of Preorganized Phosphonated Pyridines. *Inorg. Chem.* **2018**, *57*, 6095−6106.

45) Souri, N.; Tian, P.; Lecointre, A.; Lemaire, Z.; Chafaa, S.; Strub, J.-M.; Cianférani, S.; Elhabiri, M.; Platas-Iglesias, C.; Charbonnière, L. J. Step by Step Assembly of Polynuclear Lanthanide Complexes with a Phosphonated Bipyridine Ligand. *Inorg. Chem.* **2016**, *55*(24), 12962-12974.

46) Kokan, Z.; Chmielewski, M. J. A Photoswitchable Heteroditopic Ion-Pair Receptor. *J. Am. Chem. Soc.* **2018**, *140*, 47, 16010–16014.

47) Le Fur, M.; Beyler, M.; Molnar, E.; Fougere, O.; Esteban-Gomez, D.; Tircso, G.; Platas-Iglesias, C.; Lepareur, N.; Rousseaux, O.; Tripier, R., The role of the capping bond effect on pyclen $^{nat}Y^{3+}/^{90}Y^{3+}$ chelates: full control of the regiospecific N-functionalization makes the difference. *Chem. Commun.* **2017**, *53* (69), 9534-9537.

48) Le Fur, M.; Beyler, M.; Molnár, E.; Fougère, O.; Esteban-Gómez, D.; Tircsó, G.; Platas-Iglesias, C.; Lepareur, N.; Rousseaux, O.; Tripier, R. Stable and Inert Yttrium(III) Complexes with Pyclen-Based Ligands Bearing Pendant Picolinate Arms: Toward New Pharmaceuticals for β-Radiotherapy. *Inorg. Chem.* **2018**, *57*, 2051-2063.

49) Charbonnière, L.J.; Mameri, S.; Kadjane, P.; Platas-Iglesias C.; Ziessel, R. Tuning the coordination sphere around luminescent lanthanide complexes for anion sensing. *Inorg. Chem.* **2008**, *47*, 3748-3762.

50) Gampp, H.; Maeder, M.; Meyer, C. J.; Zuberbühler, A. D. Calculation of Equilibrium Constants from Multiwavelength Spectroscopic Data-II32, 95: Specfit: two user-friendly programs in basic and standard fortran 77 *Talanta* **1985**, *32* (4), 257−264.

51) Gampp, H.; Maeder, M.; Meyer, C. J.; Zuberbühler, A. D. Calculation of Equilibrium Constants from Multiwavelength Spectroscopic Data-III: Model-Free Analysis of Spectrophotometric and ESR Titrations. *Talanta* **1985**, *32* (12), 1133−1139.

52) Charbonnière, L. J.; Ziessel, R.; Guardigli, M.; Roda, A.; Sabbatini, N.; Cesario, M. Lanthanide Tags for Time-Resolved Luminescence Microscopy Displaying Improved Stability and Optical Properties *J. Am. Chem. Soc.* **2001,** *123,* 2436-2437.

53) Gillet, R.; Roux, A.; Brandel, J.; Huclier-Markai, S.; Camerel, F.; Jeannin, F.; Nonat, M.N.; Charbonnière, L.J. New bispidol chelate with phosphonate pendant arm: synthesis, Cu(II) complexation and ^{64}Cu labeling *Inorg. Chem*., **2017**, *56*, 11738-11752.

54) Mato-Iglesias, *M.;* Balogh, *E.;* Platas-Iglesias, C.; Toth, *E.;* de Blas, A.; Rodriguez Blas, T. Pyridine and phosphonate containing ligands for stable lanthanide complexation. An experimental and theoretical study to assess the solution structure. *Dalton Trans.*, **2006**, 5404**–**5415.

55) Edward, J. T. Molecular Volumes and the Stokes-Einstein Equation. *J. Chem. Educ.* **1970**, *47*, 261-270.

56) Wheate, N. J.; Kumar, P. G. A.; Torres, A. M.; Aldrich-Wright, J. R.; Price, W. S. Examination of Cucurbit[7]uril and Its Host-Guest Complexes by Diffusion Nuclear Magnetic Resonance. *J. Phys. Chem. B*. **2008**, *112*, 2311-2314.

57) Wacker, A.; Carniato, F.; Platas-Iglesias, C.; Esteban-Gomez, D.; Wester, H.-J.; Tei, L.; Notni, J. Dimer Formation of GdDO3A-arylsulfonamide Complexes Causes Loss of pH-Dependency of Relaxivity, *Dalton Trans.* **2017**, *46*, 16828-16836.

58) Nizou, G.; Molnár, E.; Hamon, N.; Kálmán, F. K; Fougère, O.; Rousseaux, O.; Esteban-Gòmez, D.; Platas-Iglesias, C.; Beyler, M.; Tircsó, G.; Tripier, R. Pyclen-Based Ligands Bearing Pendant Picolinate Arms for Gadolinium Complexation. *Inorg. Chem.* **2021**, *60* (4), 2390-2405.

59) Vander Elst, L.; Sessoye, A; Laurent, S.; Muller, R. N. Can the Theoretical Fitting of the Proton-Nuclear-Magnetic-Relaxation-Dispersion (Proton NMRD) Curves of Paramagnetic Complexes Be Improved by Independent Measurement of Their Self-Diffusion Coefficients*? Hel. Chim. Acta.* **2005**, 88, 574-587.

60) Botta M. Second Coordination Sphere Water Molecules and Relaxivity of Gadolinium(III) Complexes: Implications for MRI Contrast Agents. *Eur. J. Inorg. Chem.* **2000**, 399-407.

61) Balogh, E.; Mato-Iglesias, M.; Platas-Iglesias, C.; Tóth, E.; Djanashvili, K.; Peters, J. A.; de Blas, A.; Rodríguez-Blas, T.; Pyridine- and Phosphonate-Containing Ligands for Stable

Ln Complexation. Extremely Fast Water Exchange on the GdIII Chelates. *Inorg. Chem.* **2006**, *45*(21), 8719–8728.
62) Elhabiri, M.; Abada, S.; Sy, M.; Nonat A.; Choquet, P.; Esteban-Gomez, D.; Cassino, C.; Platas-iglesias, C.; Botta, M.; Charbonnière, L. J. Importance of outer sphere and aggregation phenomena in the relaxation properties of phosphonated gadolinium complexes with potential applications as MRI Contrast Agents. *Chem.-Eur. J.* **2015**, *21*, 6535-6546.
63) Lucio-Martínez, F.; Garda, Z.; Váradi, B.; Kálmán, F. K., Esteban-Gómez, D.; Tóth, E.; Tircsó, G.; Platas-Iglesias, C. Rigidified Derivative of the Non-macrocyclic Ligand H4 OCTAPA for Stable Lanthanide(III) Complexation. *Inorg. Chem.* **2022**, *61*, 5157−5171.
64) Blahut, J.; Hermann, P.; Tošner, Z.; Platas-Iglesias, C. A combined NMR and DFT study of conformational dynamics in lanthanide complexes of macrocyclic DOTA-like ligands. *Phys. Chem. Chem. Phys.* **2017**, *19*, 26662-26671.
65) Sherry, A. D.; Ren, J.; Huskens, J.; Brucher, E.; Toth, E.; Geraldes, C. F. C. G.; Castro, M. M. C. A.; Cacheris, W. P. Characterization of Lanthanide(III) DOTP Complexes: Thermodynamics, Protonation, and Coordination to Alkali Metal Ions. Inorg. Chem. **1996**, *35*, 4604-4612.
66) Cucinotta, G.; Peretti, M. ; Luzon, J. ; Etienne, M. ; Car, P.-E. ; Caneschi, A. ; Calvez, G ; Bernot, K. ; Sessoli, R. Magnetic anisotropy in a dysprosium/DOTA single-molecule magnet: beyond simple magneto-structural correlations. *Angew. Chem. Int. Ed.* **2012**, *51*, 1606 –1610.
67) Beeby, A.; Clarkson, I. M.; Dickins, R. S.; Faulkner, S.; Parker,D.; Royle, L.; de Sousa, A. S.; Williams, J. A. G.; Woods, M. Non-Radiative Deactivation of the Excited States of Europium, Terbiumand Ytterbium Complexes by Proximate Energy-Matched OH, NH and CH Oscillators: An Improved Luminescence Method for Establishing Solution Hydration States. *J. Chem. Soc., Perkin Trans. 2*. **1999**, 493−504.
68) Esteban-Gómez,D.; Buldt, L. A.; Perez-Lourido, P. ; Valencia, L.; Seitz, M.; Platas-Iglesias, C. Understanding the Optical and Magnetic Properties of Ytterbium(III) Complexes. *Inorg. Chem.* **2019**, *58*, 3732−3743.
69) Soro, L. K; Knighton, R. C.; Avecilla, F.; Thor, W.; Przybilla, F.; Jeannin, O.; Esteban-Gomez, D.; Platas-Iglesias, C.; Charbonnière, L. J. Solution-State Cooperative Luminescence Upconversion in Molecular Ytterbium Dimers. *Adv. Optical Mater.* **2022**, 2202307.
70) Polasek, M.; Sedinova, M.; Kotek, J.; Vander Elst, L.; Muller, R. N.; Hermann, P.; Lukes, I. Pyridine-N-oxide Analogues of DOTA and Their Gadolinium(III) Complexes Endowed with a Fast Water Exchange on the Square-Antiprismatic Isomer. *Inorg. Chem.* **2009**, *48* (2), 455-465.
71) Gottlieb, H.E.; Kotlyar, V.; Nudelman, A. NMR Chemical Shifts of Common Laboratory Solvents as Trace Impurities *J. Org. Chem.* **1997**, *62*, 7512-7515.
72) Mikkelsen K.; Nielsen, S. O. Acidity Measurements With The Glass Electrode In H_2O-D_2O Mixtures *J. Phys. Chem*. **1960**, 64 (5), 632-636.
73) Patiny, L.; Borel, A. ChemCalc: a building block for tomorrow's chemical infrastructure. *J. Chem. Inf. Model.* **2013**, *53*(5), 1223-1228.
74) Methodes d'analyse Complexometriques Avec Les Titriplex . Merck E: Darmstadt, 1990.
75) Molecular Fluorescence: Principles and Applications, 2nd Edition - Valeur, B. and Berberan-Santos, M. N. 2013, Weinheim: Wiley-VCH.
76) H. Ishida, S. Tobita, Y. Hasegawa, R. Katoh, et K. Nozaki, Recent advances in instrumentation for absolute emission quantum yield measurements. *Coord. Chem. Rev.* **2010**, 254 (21), 2449-2458.
77) Weibel, N.; Charbonnière, L. J.; Guardigli, M.; Roda, A.; Ziessel, R. Engineering of Highly Luminescent Lanthanide Tags Suitable for Protein Labeling and Time-Resolved Luminescence Imaging. *J. Am. Chem. Soc.* **2004**, *126* (15), 4888-4896.
78) Benson, R. C.; Kues, H. A. Fluorescence properties of indocyanine green as related to angiography. *Phys. Med. Biol.* **1978**, 23 (1), 159-163.
79) Frisch, M. J.; Trucks, G. W.; Schlegel, H. B.; Scuseria, G. E.; Robb, M. A.; Cheeseman, J. R.; Scalmani, G.; Barone, V.; Petersson, G. A.; Nakatsuji, H.; Li, X.; Caricato, M.; Marenich, A. V.; Bloino, J.; Janesko, B. G.; Gomperts, R.; Mennucci, B.; Hratchian, H. P.; Ortiz, J. V.; Izmaylov, A. F.; Sonnenberg, J. L.; Williams; Ding, F.; Lipparini, F.; Egidi, F.; Goings, J.; Peng, B.; Petrone, A.; Henderson, T.; Ranasinghe, D.; Zakrzewski, V. G.; Gao, J.; Rega, N.; Zheng, G.; Liang, W.; Hada, M.; Ehara, M.; Toyota, K.; Fukuda, R.; Hasegawa, J.; Ishida, M.; Nakajima, T.; Honda, Y.; Kitao, O.; Nakai, H.; Vreven, T.; Throssell, K.; Montgomery Jr., J. A.; Peralta, J. E.; Ogliaro, F.; Bearpark, M. J.; Heyd, J. J.; Brothers, E. N.; Kudin, K. N.; Staroverov, V. N.; Keith, T. A.; Kobayashi, R.; Normand, J.; Raghavachari, K.; Rendell, A. P.; Burant, J. C.; Iyengar, S. S.; Tomasi, J.; Cossi, M.; Millam, J. M.; Klene, M.; Adamo, C.; Cammi, R.; Ochterski, J. W.; Martin, R. L.; Morokuma, K.; Farkas, O.; Foresman, J. B.; Fox, D. J. Gaussian 16 Rev. C.01, 2016.
80) Tao, J.; Perdew, J. P.; Staroverov, V. N.; Scuseria, G. E. Climbing the Density Functional Ladder: Nonempirical Meta–Generalized Gradient Approximation Designed for Molecules and Solids. *Phys. Rev. Lett.* **2003**, *91* (14), 146401.
81) Dolg, M.; Stoll, H.; Savin, A.; Preuss, H. Energy-Adjusted Pseudopotentials for the Rare Earth Elements. *Theor. Chim. Acta* **1989**, *75* (3), 173–194.
82) Tomasi, J.; Mennucci, B.; Cammi, R. Quantum Mechanical Continuum Solvation Models. *Chem. Rev.* **2005**, *105* (8), 2999–3094.
83) Malmqvist, P.-Å.; Roos, B. O. The CASSCF State Interaction Method. *Chem. Phys. Lett.* **1989**, *155* (2), 189–194.
84) Neese, F. Software Update: The ORCA Program System, Version 4.0. *WIREs Comput. Mol. Sci.* **2018**, *8* (1), e1327.
85) Neese, F. The ORCA Program System. *WIREs Comput. Mol. Sci.* **2012**, *2* (1), 73–78.
86) Angeli, C.; Borini, S.; Cestari, M.; Cimiraglia, R. A Quasidegenerate Formulation of the Second Order N-

Electron Valence State Perturbation Theory Approach. *J. Chem. Phys.* **2004**, *121* (9), 4043–4049.
87) Angeli, C.; Cimiraglia, R.; Evangelisti, S.; Leininger, T.; Malrieu, J.-P. Introduction of *n* -Electron Valence States for Multireference Perturbation Theory. *J. Chem. Phys.* **2001**, *114* (23), 10252–10264.
88) Barysz, M.; Sadlej, A. J. Two-Component Methods of Relativistic Quantum Chemistry: From the Douglas–Kroll Approximation to the Exact Two-Component Formalism. *J. Mol. Struct. THEOCHEM* **2001**, *573* (1–3), 181–200.
89) Reiher, M. Douglas–Kroll–Hess Theory: A Relativistic Electrons-Only Theory for Chemistry. *Theor. Chem. Acc.* **2006**, *116* (1–3), 241–252.
90) Visscher, L.; Dyall, K. G. Dirac–Fock Atomic Electronic Structure Calculations Using Different Nuclear Charge Distributions. *At. Data Nucl. Data Tables* **1997**, *67* (2), 207–224.
91) Marenich, A. V.; Cramer, C. J.; Truhlar, D. G. Universal Solvation Model Based on Solute Electron Density and on a Continuum Model of the Solvent Defined by the Bulk Dielectric Constant and Atomic Surface Tensions. *J. Phys. Chem. B* **2009**, *113* (18), 6378–6396.
92) Maganas, D.; Sottini, S.; Kyritsis, P.; Groenen, E. J. J.; Neese, F. Theoretical Analysis of the Spin Hamiltonian Parameters in $Co^{(II)}S_4$ Complexes, Using Density Functional Theory and Correlated Ab Initio Methods. *Inorg. Chem.* **2011**, *50* (18), 8741–8754.
93) Pathak, S.; Lang, L.; Neese, F. A Dynamic Correlation Dressed Complete Active Space Method: Theory, Implementation, and Preliminary Applications. *J. Chem. Phys.* **2017**, *147* (23), 234109.
94) Weigend, F. Accurate Coulomb-Fitting Basis Sets for H to Rn. *Phys. Chem. Chem. Phys.* **2006**, *8* (9), 1057.
95) Aravena, D.; Neese, F.; Pantazis, D. A. Improved Segmented All-Electron Relativistically Contracted Basis Sets for the Lanthanides. *J. Chem. Theory Comput.* **2016**, *12* (3), 1148–1156.
96) Neese, F.; Wennmohs, F.; Hansen, A.; Becker, U. Efficient, Approximate and Parallel Hartree–Fock and Hybrid DFT Calculations. A 'Chain-of-Spheres' Algorithm for the Hartree–Fock Exchange. *Chem. Phys.* **2009**, *356* (1–3), 98–109.
97) Izsák, R.; Neese, F. An Overlap Fitted Chain of Spheres Exchange Method. *J. Chem. Phys.* **2011**, *135* (14), 144105.
98) Neese, F. An Improvement of the Resolution of the Identity Approximation for the Formation of the Coulomb Matrix. *J. Comput. Chem.* **2003**, *24* (14), 1740–1747.
99) Stoychev, G. L.; Auer, A. A.; Neese, F. Automatic Generation of Auxiliary Basis Sets. *J. Chem. Theory Comput.* **2017**, *13* (2), 554–562.

TOC graphic and Synopsys text

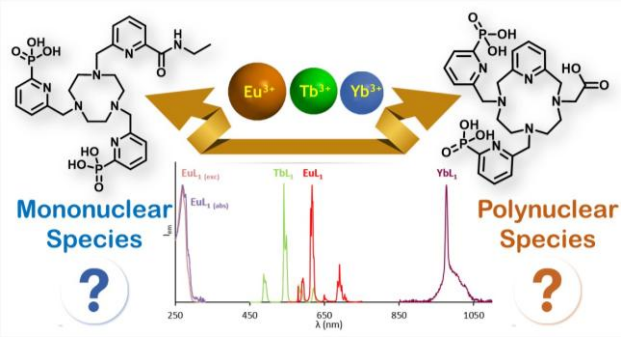

L1 and **L2**, two tacn- or pyclen-based chelators with pyridinylphosphonic arms have been synthesized to investigate their coordination properties towards lanthanide ions. Both generate new monomeric and polymeric species with a very good shielding of the cation in the monomeric one.